# COMETARY DUST

ZDENEK SEKANINA, MARTHA S. HANNER
*Jet Propulsion Laboratory, California Institute of Technology*

ELMAR K. JESSBERGER
*Institut für Planetologie, Westfälische Wilhelms-Universität Münster*

and

MARINA N. FOMENKOVA
*Center for Astrophysics and Space Sciences,*
*University of California San Diego*

This chapter reviews the history of cometary dust investigations. The individual sections describe the progress achieved in the understanding of the dynamical properties of cometary dust, its optical, thermal, and other physical properties, and its chemistry. The review emphasizes information that was obtained during the three recent major observing campaigns, focussed on comets 1P/Halley, Shoemaker-Levy 9 (1994 X = D/1993 F2), and Hale-Bopp (C/1995 O1). Where appropriate, the review relates the discussed topics to relevant issues of cometary nuclei and their physical and chemical properties.

## 1. INTRODUCTION

Since the most recent encyclopedic review of the problems of cosmic dust, in a book edited by McDonnell (1978), three major events have occurred that have greatly contributed, and still are contributing, to our much increased knowledge of comets in general and of cometary dust in particular. One of the events was a long awaited one, while the other two have been entirely unexpected. We refer, of course, to the return of comet 1P/Halley in 1986, to the most peculiar cometary object ever observed, Shoemaker-Levy 9 (1994 X = D/1993 F2), in 1993-94, and to comet Hale-Bopp (C/1995 O1), one of the most spectacular comets of all time, which was discovered in 1995 and is still under observation at the time of this writing.

Among the highlights from observations of Halley's comet, at least four that involve dust should be listed at the outset: (i) first direct information was obtained on the chemistry of cometary particles, (ii) first evidence was gathered on attogram grains, which bridge the gap be-

tween molecules and particulates, (iii) a pre-1986 inference, from morphological studies of a number of comets, that dust ejection is confined to relatively small, isolated active areas on the sunlit side of the nucleus was spectacularly confirmed by closeup imaging from onboard the intercepting spacecraft, and (iv) a major outburst of dust was detected at a record heliocentric distance of 14 AU after perihelion.

The greatest contributions from Shoemaker-Levy 9's observations to our understanding of cometary dust are in the areas of (i) mechanical strength of cometary material (or, rather, the lack thereof), (ii) fragmentation processes both in interplanetary space and upon the object's entry into the Jovian atmosphere, and (iii) physical and chemical interactive atmospheric processes triggered during and after each fragment's penetration into the atmosphere.

The ongoing investigations of comet Hale-Bopp provide a wealth of new information in a number of research areas on cometary dust, including huge amounts of invaluable data on coma morphology, on thermal properties and composition of grains, and on processes of dust emission at large heliocentric distances. Most of these studies are still in progress, some have just barely begun.

In the following the discussion of cometary dust is divided into three broad categories: (i) its dynamical properties, (ii) its physical properties, including the optical and thermal ones, and (iii) its chemistry. Because of constraints of space, not discussed are the problems of cometary contributions to maintaining the interplanetary dust cloud and relevant implications for studies of cometary dust from laboratory experiments.

## 2. DYNAMICAL PROPERTIES

Historically, the early efforts that led to information on cometary dust began with Bessel's (1836) pioneering work on the coma morphology of Halley's comet at its 1835 apparition, in which he introduced the concept of a repulsive force from the Sun. The progress continued with Bredikhin's independent studies of tail formation in the late 19th century (for a review, see Jaegermann 1903). Bredikhin is responsible for two additions to cometary terminology that are still extensively used today to describe the dust tails: a *syndyname* (or *syndyne*) as a locus of particulates that are subjected to a constant acceleration by the repulsive force and a *synchrone* (or *isochrone*) as a locus of particulates that are ejected from the comet at the same time. The repulsive force was identified as *solar radiation pressure* at the break of this century (Arrhenius 1900, Schwarzschild 1901), although Norton (1844) pointed out that L. Euler had already considered the possibility that the repulsive force "consists in an impulsive action of the sun's rays." For dust tails, this interpretation has universally been accepted.

## 2.1. Ejection and Motion of Dust Grains

Based on Whipple's (1950) icy-conglomerate model, a consensus has developed that dust particulates are released from the cometary nucleus and accelerated to their "terminal" velocities by drag forces exerted by the sublimating ice, with which the refractive material is mixed in cometary nuclei and on their surface. The terminal velocity is reached when the grain becomes dynamically decoupled from the expanding gas, that is, when particle-molecule collisions are no longer dynamically significant. As the gas drag drops, solar radiation pressure becomes, next to solar attraction, the dominant force on most dust particles that are observed. And since the acceleration due to solar attraction affects the motions of dust and the nucleus equally, the motion of a particle relative to the nucleus is determined by solar radiation pressure alone, unless additional (usually minor) nongravitational forces are involved.

### *2.1.1. Gas-dust interaction and particle ejection velocities*

A simple formula derived from the equation of motion involving the drag force was given by Whipple (1951), who assumed that the drag coefficient and the gas velocity were constant in the gas-dust interaction zone. This formula was more recently generalized to nonspherical shapes by Gustafson (1989).

The first elaborate treatment of the problem of dusty gasdynamics in comets was presented by Probstein (1969), who used a free molecular approximation to describe the gas flow and solved the equation of motion for a dust particle together with the relevant conservation equations for the dusty gas flow's mass, momentum, and energy. Probstein demonstrated that the drag coefficient is primarily a function of the Mach number and the specific heat ratio of the gas. For assumed perfect thermal accommodation between gas and dust and for a *single* characteristic grain size, he obtained transonic solutions for the accelerating gas flow, with the terminal velocity of dust particles reached within ~20 radii of the nucleus (where gas and dust essentially decouple), depending on the dust loading of the gas and on the accommodation coefficient. This coefficient varies as the product of a dust particle's size and bulk density, the nucleus radius, and the thermal velocity of the gas, and inversely as the mass flow rate of the gas. At an assumed gas temperature of 200 K, Probstein's results yield dust terminal velocities for submicron-sized grains that converge to 0.74 km/s when the dust loading of the gas flow is negligibly low, to 0.57 km/s when the dust and gas mass flows are equal, and to 0.36 km/s when the dust mass flow exceeds the gas mass flow by a factor of 10. Probstein's two-component solution to the gas-dust interaction was incorporated as an essential component of the Finson-Probstein analysis of the dust tails of comets (Sec. 2.3.1).

A stringent test of Probstein's results was provided by subsequent studies of the gradual expansion of distinct dust features in the heads of comets 109P/Swift-Tuttle (Sekanina 1981a) and 1P/Halley (Sekanina and Larson 1984, 1986a) at heliocentric distances near 1 AU. The ejection velocities (equal to Probstein's terminal velocities) of submicron-sized particles were found to vary between 0.4 and 0.7 km/s, in excellent correspondence with the theory. Fitting Probstein's theoretical curves led to a suggestion (Sekanina 1981a) that the relationship between the ejection velocity $v_{\rm eject}$ of a dust particle and the solar radiation pressure acceleration $\beta$ to which the particle's motion is subjected (Sec. 2.1.2) could be approximated by a simple empirical formula:

$$v_{\rm eject} = \frac{a}{1 + b/\sqrt{\beta}}, \tag{1}$$

where $a$ and $b$ are coefficients expressible in terms of the physical parameters of Probstein's theory.

In spite of the apparent agreement between theory and observation, some aspects of Probstein's treatment (assumption of a single characteristic grain size, oversimplified energy conservation equation, neglect of molecule-molecule collisions near the nucleus, etc.) were found by others to be unrealistic enough to warrant numerous refinements in, and innovations to, Probstein's original approach (e.g., Hellmich 1981, Hellmich and Keller 1981, Marconi and Mendis 1983, 1984, Gombosi et al. 1983, 1985, Gombosi 1986; cf. also a review by Crifo 1991), but these efforts led to no dramatic changes in the determination of the terminal velocities of dust particles. Applications of hydrodynamic models to emission scenarios involving localized jets are discussed in Sec. 2.2.2.

*2.1.2. Dust acceleration by solar radiation pressure*

The acceleration that solar radiation pressure exerts on dust particles in comets is commonly expressed in units of the acceleration by solar attraction at the same heliocentric distance. This dimensionless ratio, in the current literature usually called $\beta$, varies as the particle's projected cross sectional area $A$ and inversely as its mass $m$:

$$\beta = \frac{Q_{\rm pr} L_\odot A}{4\pi c G M_\odot m}, \tag{2}$$

where $c$ is the speed of light, $G$ is the gravitation constant, $M_\odot$ and $L_\odot$ are the Sun's mass and total energy emitted per second, and $Q_{\rm pr}$ is the radiation pressure efficiency for the particle, which depends on its size, shape, and optical properties. A large number of studies exist that are dedicated to calculations of $Q_{\rm pr}$ and $\beta$ and their variations with particle size. Most of these investigations employ the Mie theory and refer to compact spherical grains of particular compositions (e.g., Schwehm and

Rohde 1977; Burns et al. 1979), but some also consider models of core-mantle particles (Schwehm 1976) and particles that are composed of mixtures of materials (Lien 1991). Generally, for a spherical particle of radius $a$ (in $\mu$m) and density $\rho$ (in g/cm$^3$) we have

$$\beta = \frac{0.574\, Q_{\rm pr}}{\rho a}. \tag{3}$$

The principal results of these calculations are major differences between the values of $\beta$ for absorbing (such as carbon-rich or metallic) grains on the one hand and for dielectric (such as glassy, basaltic, or icy) particles on the other hand. Absorbing grains have a peak $\beta$ value greater than unity (for example, $\sim$1.8 for iron, $>$5 for graphite) at a particle radius near 0.1 $\mu$m; for extremely tiny grains ($<$0.01 $\mu$m) the $\beta$ value converges to a nonzero constant. By contrast, dielectric grains have a peak $\beta$ value smaller than unity (mostly near 0.5–0.6) at a particle radius near 0.2–0.3 $\mu$m and very tiny particles of this kind are virtually transparent to light, having $\beta \sim 0$.

The intermediate critical value, $\beta = 1$, has a very simple and fundamental meaning. Such particles are subjected to solar radiation pressure that balances solar gravity, so that they move through the solar system with constant velocities along straight lines. For $\beta < 1$ the orbit may be either an ellipse or a concave hyperbola, depending on the motion of the parent comet. If the comet's orbit is a parabola, then the orbit of a particle released with no impulse is a hyperbola. For $\beta > 1$, a particle's orbit is always a convex hyperbola, regardless of the parent comet's motion.

Observations indicate that, except for antitails (Sec. 2.3.3), a peak radiation pressure acceleration on dust particles in comets is typically $\beta_{\rm peak} \simeq 2.5$, including grains in streamers (Sec. 2.3.2) and striae (Sec. 2.3.4) (e.g., Orlov 1960, Sekanina and Farrell 1980, 1982, Sekanina 1981b, 1986, Akabane 1983, Lamy 1986a, Beisser and Boehnhardt 1987a, b, Notni and Thänert 1988, Nishioka and Watanabe 1990).

### *2.1.3. Motions of charged grains*

It is generally recognized that because of their interaction with the radiative and plasma environment, dust particles in cometary heads and tails must be electrostatically charged. The grain charging depends on the physical and electrical properties of the grains, on the nature of their interaction with the surrounding radiation and plasma fields, and on the relative velocity. The most important contributions come from a flux of electrons and ions, from UV-radiation induced photoemission, and from secondary emission of electrons.

The process of electrostatic charging on cometary dust particles and the equilibrium potentials to which they are expected to be charged have extensively been discussed in the literature (e.g., Notni 1964, 1966;

Boehnhardt 1986; Horányi and Mendis 1986; Boehnhardt and Fechtig 1987; Notni and Tiersch 1987; Tiersch and Notni 1989). The results indicate that the potential is usually only a few volts; it is positive in cases involving high photoelectron currents, negative in a high plasma-density environment. Boehnhardt and Fechtig (1987) find that, during the spacecraft encounters, silicate grains in 21P/Giacobini-Zinner and 1P/Halley carried a positive charge of up to 10 volts outside the cometopause, whereas the electrostatic potential of carbon-rich grains varied strongly with the plasma environment conditions, reaching both positive and negative values. Near the nucleus, the potential was negative but very low (~0.1 volt).

There are two important effects that charged particles are subjected to: electrostatic fragmentation (cf. Sec. 2.3.4) and interaction with the interplanetary magnetic field. Boehnhardt (1986) and Boehnhardt and Fechtig (1987) conclude that only small and fluffy dust particles (0.1 to 1 $\mu$m in size and of a tensile strength of 0.001 to 0.01 bar) can be broken up electrostatically in comets. Even though there is an indication, primarily from examined events of cometary splitting, that on large scales the tensile strength of cometary nuclei is in the required range (e.g., Sekanina 1982a, 1996a; Greenberg et al. 1995), the situation on microscopic scales is far less clear and evidence for electrostatic fragmentation remains inconclusive.

The interaction of a charged dust particle with the interplanetary magnetic field leads to the generation of a Lorentz force. The acceleration of a spherical particle of radius $a$ and density $\rho$ by the Lorentz force is

$$\mathbf{L} = \frac{3\epsilon_0 \Phi}{\rho a^2} [(\mathbf{v} - \mathbf{w}) \times \mathbf{B}], \tag{4}$$

where $\epsilon_0$ is the permittivity constant, $\Phi$ is the equilibrium electrostatic potential, $\mathbf{v}$ is the vector of the particle's velocity relative to the Sun, $\mathbf{w}$ is the vector of the solar-wind velocity, and $\mathbf{B}$ is the interplanetary magnetic field's strength. In analogy to the dimensionless quantity $\beta$ for the radiation pressure acceleration (Sec. 2.1.2), one can express the acceleration by the Lorentz force by a dimensionless quantity $\gamma$, in units of the acceleration due to solar attraction. Applying Parker's (1958, 1963) model of the axially symmetric, quiet-day interplanetary magnetic field, the ratio $\gamma$ is equal to

$$\gamma = \frac{0.447\, \Phi \kappa B_{\rm rad}}{\rho a^2}, \tag{5}$$

where $a$ is in $\mu$m, $\rho$ in g/cm$^3$, and $\Phi$ in volts, $B_{\rm rad}$ (in gauss) is the radial component of the magnetic field at a heliocentric distance of 1 AU, and $\kappa$ is a function of the vector product in Eq. (4). When $||\mathbf{w}|| \gg ||\mathbf{v}||$, as is almost universally the case, then $\kappa \approx \Omega\, r \cos b$, with $\Omega$ being the Sun's

angular rotation velocity (in $s^{-1}$), $r$ the comet's heliocentric distance (in km), and $b$ its heliographic latitude.

There are two major differences between effects of the Lorentz force and radiation pressure on a dust particle's motion: (i) the Lorentz acceleration ratio $\gamma \propto a^{-2}$, whereas, in the first approximation, the radiation pressure acceleration ratio $\beta \propto a^{-1}$, so that effects of electrostatic charging should become the more important the smaller the particle; and (ii) unlike radiation pressure, the Lorentz force contributes a nonzero component in the direction normal to the comet's orbital plane.

Effects of particle charging on the motion of cometary dust have not been subjected to systematic tests. From the fact that solar radiation pressure adequately accounts for the motions of striae (Sec. 2.3.4) in the dust tail of comet West (1976 VI = C/1975 V1), Sekanina and Farrell (1980) estimated that submicron particles that made up the features could not be charged to potentials higher than a few volts at the most. An apparent signature, in the tail of comet SOLWIND 1 (1979 XI = C/1979 Q1), of the interaction of charged dust with the coronal magnetic field of the Sun (Sekanina 1982b) is likely to be invalidated by a more recent revision of the object's positional observations and orbital elements (Marsden 1989). At present, the strongest evidence against detectable effects of electrostatic charging on the motion of cometary dust comes from incidental observations during the Earth's transits across the orbital planes of comets. Such episodes are common, taking place twice a year for every object, and they are virtually continuous occurrences for comets of a very low orbit inclination (a significant fraction of the short-period comets). In spite of the omnipresence of such events, no instance is known of a dust-tail orientation out of the orbital plane, which at the time of Earth's transit projects as the great circle in a predictable position angle.

## 2.2. Dust Features in Cometary Heads

Information on structural detail in the heads of comets has slowly been accumulating over centuries. It appears that the first observation of a distinct coma feature, clearly documented in the literature, is that of Halley's comet by Hevelius (1682) on September 8, 1682. The drawing, displaying a bright curved jet near the nucleus, predates E. Halley's discovery of the object's orbital periodicity by 13 years. Numerous graphical renditions of dust features in dozens of comets — some of them accompanied by micrometric measurements — were published during the 19th century. Examples of these drawings were reproduced by Rahe et al. (1969). As photography was gradually replacing visual telescopic observations of comets in the late 1800s and the early 1900s, the amount of new information on coma morphology began to decrease. The renewed interest in the subject since the 1970s has been motivated primarily by

the development of sophisticated computer-processing techniques that allow digital enhancement of structural detail on available images and by major advances in detector performance, especially the availability of the charge coupled device (CCD) arrays. Also instrumental in these revitalization efforts was the pressing need for a better understanding of the nucleus environment in the era of space exploration of comets.

*2.2.1. Nucleus rotation and discrete emission sources*

Growing evidence for nucleus rotation and for the presence of discrete emission sources on the nucleus surface was one of the factors that contributed to the broad acceptance of the icy conglomerate model in the 1970s. These pioneering efforts were based in part on old visual observations of nearly concentric halos in the head of comet Donati (1858 VI = C/1858 L1) by Whipple (1978). By then, Larson and Minton (1972) (cf. also Larson 1978) had already derived the rotation period of comet Bennett (1970 II = C/1969 Y1) from separations in a system of spiral jets, observed photographically in its dust coma. At about the same time, independent efforts were in progress, aimed at determining the position of the nuclear spin axis from projected orientations of dust features (such as jets, fans, or spirals) and their motions in the coma (Sekanina 1979, 1981a). An attempt was even made to establish precession of comet 2P/Encke (Whipple and Sekanina 1979). A review of the early morphological studies of cometary dust (Sekanina 1981c) confirmed that outgassing from many, especially short-period, comets is indeed largely confined to discrete areas on the sunlit side of their rotating nuclei and that the appearance of the observed features is determined by the surface distribution of the sources and by the emission mode (continuous vs. erratic) and insolation regime (circumpolar Sun vs. day-and-night). Even though it has more recently been recognized that Halley's state of rotation is more complicated than originally thought, the closeup images of this comet's nucleus — particularly those taken with the Giotto's Halley Multicolor Camera (Keller et al. 1987) — fully confirm the earlier conclusion that dust emanations from the nucleus are largely restricted to isolated sources situated on its sunlit side.

*2.2.2. Hydrodynamic models for dust emission from discrete sources*

Following Halley's apparition of 1986, significant progress has been achieved in the understanding of the outflow mechanism and the thermophysical properties of gas and dust emissions that expand from the nucleus in a highly anisotropic fashion. Observations of several comets, including 1P/Halley and 2P/Encke, show that both the radio and the UV spectra of OH exhibit significant asymmetries in the line-of-sight velocity profiles (e.g., Snyder et al. 1976, Bockelée-Morvan and Gérard 1984, de Pater et al. 1986, A'Hearn and Schleicher 1988).

Stimulated by the closeup appearance of Halley's nucleus and its environment, efforts aimed at formulating axisymmetric hydrodynamic models that offer dynamical solutions for an anisotropic flow of gas and/or dusty gas from a localized active area got underway in the late 1980s (Kitamura 1986, 1987; Kömle and Ip 1987a, b; Körösmezey and Gombosi 1990). The Kitamura and Kömle-Ip models were reviewed by Kömle (1990), while the Kitamura and the Körösmezey-Gombosi models were discussed by Gombosi (1991). These models begin with the mass, momentum, and energy conservation equations for perfect gas and with the continuity and energy balance equations for the dust particles entrained in the gas flow. Some of the more interesting results from these calculations include, according to Körösmezey and Gombosi, the formation of a dust spike and a jet cone, where much of the ejecta is contained. The spike is a combined effect of gas heating by hot dust grains above the source and of the absence of a lateral expansion velocity component along the emission axis itself (in the idealized case of an axisymmetric flow). The cone is a product of the gas pressure vectorial distribution near the nuclear surface outside the jet's axis. Keller and Thomas (1989) conclude that a near-surface "breeze," a lateral transport of material from the source toward the nightside along the pressure gradients strongly increases the dust density in the anti-sunward direction and thereby decreases the sunlit/dark brightness asymmetry. Keller et al. (1990) point out that an important role is apparently played by dust particle fragmentation almost immediately after release from the nucleus. It causes an increase in the sublimation rate from the just generated distributed source as well as a rapid mass loading of the gas flow, thereby slowing down the flow's expansion acceleration, enlarging the subsonic region, and facilitating the near-surface breeze in side directions. A breeze is predicted by the Kitamura and Körösmezey-Gombosi models. However, it is emphasized by Gombosi (1991) that the transport of dust toward the dark side is more pronounced in the models for strong jets that create a lateral shock and lead to the formation of dust cones on the dark side due to emission from a source on the sunlit side. The conclusion is that the assumption of activity from isolated sources located *only* on the sunward side of the nucleus is fully compatible with all observed near-nucleus phenomena.

*2.2.3. Expansion of dust ejecta through the coma of a rotating comet*

The hydrodynamic models describe the evolution of a dust jet in its very early stages and they disregard rotation of the nucleus. Once the interaction between the dust and the expanding gas ceases, the particulate ejecta expand through the coma under the effects of solar attraction and solar radiation pressure (described in Sec. 2.1.2). On time scales of hours and days, the nuclear rotation has dramatic effects on the distribution of dust in the coma and thereby on coma morphology.

As observed from Earth, large amounts of freshly ejected dust are first detected as a sharp central condensation or a "false" nucleus, caused by limited seeing. Next usually comes the development of a spiral jet that "unwinds" on the sunward side of the coma from the gradually fading condensation. Sometimes, however, one observes a halo instead, which is entirely separated from the condensation. The feature, whether a spiral or a halo, subsequently evolves into a slowly expanding envelope, whose surface brightness decreases with time until it vanishes completely. The feature's period of visibility is often long enough to notice its being swept into the tail on one or both sides of the nucleus.

In a special case of a point-like emission region located in the nucleus equatorial plane that coincides with the comet's orbit plane, the cometocentric motion of a dust particle ejected with a constant velocity $v_{\rm eject}$ (identified with its "terminal" velocity due to momentum exchange with expanding gas in the early post-ejection period of time) and subjected to a constant acceleration $g$ due to solar radiation pressure is described by the rectangular equatorial coordinates $x, y$, oriented, respectively, toward the Sun and 90° ahead of it in the direction of rotation (Sekanina and Larson 1984):

$$x(t,\Theta) = f(t,\Theta)\,[v_{\rm eject}\cos\Theta - \frac{1}{2}\,g\,f(t,\Theta)]$$

$$y(t,\Theta) = f(t,\Theta)\,v_{\rm eject}\sin\Theta, \qquad (6)$$

where $P$ is the rotation period, $\Theta$ is the angle of ejection, reckoned from the sunward direction in the sense of rotation and measured in radians, and

$$f(t,\Theta) = (t - t_{\rm b}) - \frac{P}{2\pi}(\Theta - \Theta_{\rm b}), \qquad (7)$$

with $t_{\rm b}$ and $\Theta_{\rm b}$ being the time and ejection angle at the onset of emission (at sunrise). Equations (6) hold for any time $t \geq t_{\rm b}$, but the function $f(t,\Theta)$ is defined only for emission during one rotation, that is, for $\Theta_{\rm b} \leq \Theta \leq \Theta_{\rm e}$, where $\Theta_{\rm e}$ is the ejection angle at the end of emission (at sunset).

The striking effect of the spin rate on the observed morphology is exemplified in Fig. 1, which shows a pole-on view of the evolution of a feature made up of dust particles ejected continuously with a constant velocity from an equatorial source between sunrise and sunset. When the nucleus spins fast, the feature soon separates from the central condensation, so that the spiral-jet phase of development has a very short duration. Several rotations after the onset of emission, a system of fairly symmetrical, almost semicircular and approximately concentric envelopes sets off. Their outlines are eventually distorted

by directionally nonuniform expansion. Particulates of identical dynamical properties ejected from a slowly rotating nucleus first form a spiral jet, which gradually evolves into a highly asymmetrical envelope. Thus, whether one observes a spiral or a halo depends strongly on the nuclear spin rate.

It is similarly possible to demonstrate effects of the inertial position of the nuclear spin axis on both the activity regime and the resulting dust coma morphology. In particular, comprehensive analysis of a variety of scenarios makes it possible to explain the distinction between fans and jets, as shown in the next subsection.

*2.2.4. Conceptual models and computer simulation of dust features*

Serious attempts to analyze, model, and interpret large-scale morphology of cometary dust atmospheres began only in the late 1970s and the early 1980s. Restricted initially to fitting contours of observed features (e.g., Sekanina and Larson 1984, 1986a, b), this work subsequently developed into an increasingly sophisticated Monte Carlo image simulation procedure (Sekanina 1987a, b, 1991a, 1996b).

Closeup images of Halley's nucleus, particularly those taken with the Giotto's camera, convincingly document dust jets streaming away from discrete sources on the sunlit side of the nucleus (Keller et al. 1987). This scenario was originally proposed for 1P/Halley by Sekanina and Larson (1984), who applied their computer simulation model to the comet's ground-based images in 1910. More recently, the model's parameters — which include the nucleus spin vector at the time of dust emission, the surface distribution of dust sources, and the range of particle ejection velocities and solar radiation pressure accelerations — were expanded to introduce random noise into synthetic images (Sekanina 1991b) to account for effects of both physical nature (such as dispersion in the vector field of particle expansion velocities) and incidental nature (such as imperfect seeing). The inclusion of noise substantially enhances the model's capability to simulate faithfully the observed coma appearance of dust comets. In addition, by increasing noise it is possible gradually to "erase" any morphological feature in the computer-generated images, as is illustrated in Fig. 2 for a system of sunward, nearly concentric halos (displayed e.g. by comet Donati C/1858 L1 and very recently by comet Hale-Bopp C/1995 O1). This possibility to erase a feature implies that large-scale morphology of a comet's head indeed is a product of collimation of dust particle flow from discrete sources, but that the lack of morphology is not necessarily an indicator of the absence of such isolated sources.

Very recently, the Monte Carlo image simulation model was further upgraded. It can now accommodate a great variety of particle size distribution laws and account for short-term (diurnal) variations in the production rate of dust from a rotating source (Sekanina 1993). This

new capability is particularly helpful when one models rapidly changing morphological features associated with sudden dust bursts.

The experience with the image simulation experiments achieved so far should serve as the basis for assessing the future of Monte Carlo modeling investigations into dust coma morphology. On the one hand, the technique, even though essentially trial-and-error in nature, is powerful enough to provide, with fairly restricted sets of reference parameters, an impressive match to extremely diverse jet patterns. On the other hand, the possible existence of multiple solutions, which may lessen the merits of the image simulation technique, is clearly of concern. Luckily, it turns out that short-term variations in dust coma morphology represent a major discriminating factor of immense diagnostic value. The significance of this time-lapse approach is particularly well demonstrated in two very recent investigations of morphological features displayed by the dust coma of comet Hale-Bopp (C/1995 O1). One of these studies (Sekanina 1998) offers a quantitative, dynamically attractive interpretation for the diurnal evolution of a dust jet observed in late February 1997 throughout one rotation period of the comet (Fig. 3) and describes the jet's transformation into a system of halos on a time scale of several rotations. The other study (Sekanina and Boehnhardt 1998) presents a conceptually innovative model for the comet's porcupine-like appearance during much of 1996.

*2.2.5. Dust emission at large heliocentric distances*

The statement, often copied in astronomical textbooks, that cometary activity is confined only to small distances from the Sun ($< 2$–$3$ AU) is demonstrably incorrect. The first comet that has repeatedly been found active at heliocentric distances exceeding 5 AU is 29P/Schwassmann-Wachmann 1. While this object can most appropriately be characterized as having continuous activity on which sporadic outbursts are superimposed (Jewitt 1990), isolated flare-ups appear to be the most conspicuous mode of activity for comets far from the Sun.

Since the problem of activity at large distances from the Sun is too broad to discuss here all of its aspects, we focus in the following on two events: an isolated outburst of 1P/Halley at 14 AU from the Sun after perihelion and the quasi-recurring flare-ups of comet Hale-Bopp (C/1995 O1) at 6–7 AU before perihelion. Both comets have perihelion distances of less than 1 AU. A morphological and photometric study of P/Halley's slowly expanding, crescent-shaped halo at 14 AU suggested that the feature represented a segment of a conical surface populated by particulate ejecta that had been released from a suddenly activated source on the sunlit side of the nucleus (Sekanina et al. 1992). The ejecta's total mass was estimated at $\sim 10^{12}$ g or more and carbon monoxide was suggested as the most likely driver, accelerating the smallest grains ($\sim 1 \mu$m across) to a terminal velocity of $\sim 45$ m/s.

The general scenario is not dramatically different for the recurring bursts of comet Hale-Bopp, even though they took place closer to the Sun and before perihelion. The comet's characteristic appearance during three major events in August–October 1995 consisted of a radial, rectilinear jet that emerged from the nucleus condensation to the northwest and turned abruptly to the east at a distance of several seconds of arc from the center, terminating as a gradually fading spiral arm that vanished in the first quadrant. These features were successfully modeled (Fig. 4) as products of sharply peaking dust injection episodes originating from an isolated source on the nucleus and lasting only a quarter of the rotation cycle (Sekanina 1996c). The peak particle expansion velocities were found to amount to 50 m/s and the total mass of the dust ejected during each event was estimated at a few times $10^{11}$ g, significantly exceeding the measured production rate of carbon monoxide, the apparent driver for the dust (e.g., Jewitt et al. 1996).

An interesting characteristic of the emission episodes experienced by P/Halley and Hale-Bopp at large distances from the Sun appears to be a very high mass loading of the CO gas flow by the dust, estimated at $\gg 10$. It remains to be seen whether this is a common property of comets.

## 2.3. Dust Tails and Their Structure

Dust tails are in most astronomical textbooks described as being structureless. This is not universally true, although their structure cannot compete with prominent features that are so characteristic of plasma tails. Dust tails are also said to be moderately curved, with a sharp leading boundary and a more diffuse trailing boundary. Again, this is often, but by no means always, the case. For extracting information on a comet's activity from its dust tail, the two-dimensional distribution of light and any evidence of morphology are the tail's most important attributes, although its orientation and approximate length and width are in some cases also highly diagnostic, as will be shown in Sec. 2.4.4.

### *2.3.1. Dust tail formation and its analysis*

The fundamental point about dust tails of comets is that it takes some, often a long, time for them to form. As a result, the history of a comet's dust emission is imprinted and preserved in its dust tail for a limited period of time. One can take advantage of this fact and recover much of the information if he knows how to "read" the tail. Additional benefits of having this kind of opportunity stem from the circumstance that the recovered information may, and often does, refer to times when the comet was not under observation, either because it was not yet discovered or because it was located too close to the Sun in the sky to be observable.

Because of the dominance of the intervening effects of solar radiation pressure, the initial conditions — such as the emission anisotropy — become of secondary importance in studies of dust tails and, with rare exceptions, have been neglected: even some of the most refined models assume that dust emission is spherically symmetrical. The three fundamental parametric functions determining the distribution of light in a dust tail are the primary objectives of the modeling efforts: (i) the mass production rate of dust particles and its temporal variations, (ii) the distribution function of the acceleration ratio $\beta$, which is closely related to the particle size and mass distribution functions, and (iii) the particle ejection velocity and its temporal variations.

The history of sophisticated dust tail modeling is brief. It began with a pioneering work by Finson and Probstein (1968a), which treats dust tails as continuous particle-flow phenomena, is based on the concept of synchrones and syndynames, and adopts Probstein's (1969) fluid-dynamic model for the interaction between gas and dust near the nucleus. This model essentially integrates contributions from superimposed uniformly expanding shells (because of finite ejection velocities) of particulates that were ejected at various times and subjected to a variety of radiation pressure accelerations, calculates the projected spatial distribution of scattered sunlight in the tail, and varies the three parametric functions until a satisfactory match has been found between the observed and modeled isophotes. In its original version this model was applied to comets Arend-Roland (1957 III = C/1956 R1) by Finson and Probstein (1968b), to comet Bennett (1970 II = C/1969 Y1) by Sekanina and Miller (1973), and to comet Seki-Lines (1962 III = C/1962 C1) by Jambor (1973).

Kimura and Liu (1977) modified the Finson-Probstein approach by introducing the concept of a "neckline" and abandoning the approximation by *uniformly* expanding shells. They argued that any particle ejected before perihelion with a finite velocity component normal to the comet's orbital plane passes through the same plane again after perihelion. If Earth should transit the comet's orbital plane at the same time as these particles, a neckline structure would be observed. This suggestion is identical with the idea suggested more than one decade earlier by Southworth (1963, 1964). Further improvements of the Finson-Probstein method were proposed by Richter and Keller (1987) and by Fulle (1987a), who also developed an independent Monte Carlo approach and examined the roles of emission asymmetry and a Maxwellian distribution of ejection velocities (Fulle 1989, 1992). Fulle and his collaborators proceeded with applications of these innovative techniques to images of dust tails of comets Halley (1986 III = 1P/1982 U1) (Fulle 1987b, Fulle et al. 1987, 1988, Cremonese and Fulle 1989), Bennett (1970 II = C/1969 Y1) (Pansecchi et al. 1987, Fulle 1987c, Fulle and Sedmak 1988), Arend-Roland (1957 III = C/1956 R1) and Seki-Lines

(1962 III = 1962 C1) (Fulle 1988a), Kohoutek (1973 XII = C/1973 E1) (Fulle 1988b), 1910 I = C/1910 A1 (Pansecchi and Fulle 1990), Wilson (1987 VII = C/1986 P1) (Cremonese and Fulle 1990), Liller (1988 V = C/1988 A1) (Fulle et al. 1992), Austin (1990 V = C/1989 X1) (Fulle et al. 1993a), Grigg-Skjellerup (1992 XVIII = 26P) (Fulle et al. 1993b), and Swift-Tuttle (1992 XXVIII = 109P/1992 S2) (Fulle et al. 1994). These techniques provide very satisfactory results for dust tails with a smooth light distribution or when they exhibit a neckline structure or an antitail (Sec. 2.3.3). They are less suitable for analysis of some of the discrete dust features that are discussed next.

*2.3.2. Streamers as indicators of outbursts*

Major but brief enhancements of dust production are brought about by cometary outbursts. The problem of outbursts and their mechanisms are outside the scope of this review and the reader is referred to numerous papers in which these topics are addressed and/or summarized at some length and from different standpoints (e.g., Hughes 1991, Sekanina 1991a, Rettig et al. 1992, Sekanina et al. 1992). Ejecta released during an outburst may display a variety of features, depending on the ejection circumstances, the heliocentric distance, and the time elapsed between the outburst and observation. If solar radiation pressure has long enough been the dominant force so that most ejecta from the outburst have reached the tail, they become observed as a discrete band or ray called here a streamer.

There is always one streamer per outburst. The streamers have the following properties: (i) they are issued from the nucleus in directions that deviate perceptibly from the extended radius vector toward the negative orbital-velocity vector; (ii) they are usually rather narrow, sometimes slightly cone-shaped, and either rectilinear or moderately curved; and (iii) as a rule, they number no more than several at a given time, all converging to the nucleus, subtending distinct angles with one another. The position angle of each streamer is diagnostic of the time of outburst, while its length provides information on the peak radiation pressure acceleration to which the ejecta were subjected. Unfortunately, streamers have a tendency to fade rapidly with time and since their brightness decreases with increasing distance from the nucleus, their observed length usually provides only a lower bound to the peak radiation pressure effect.

The dynamical behavior of particles that left the comet simultaneously was first considered by Norton (1861), who already pointed out that such particles should be distributed in the tail along a nearly straight line that points approximately at the nucleus. On the other hand, Bredikhin classified streamers as type III tails, which he regarded to be syndynames (Jaegermann 1903). Comet 1901 I (= C/1901 G1), the last studied by him, became later instrumental in bringing about

the first major modification to his classification. Moiseyev (1925) found that the streamers were synchrones and, subsequently, Orlov (1928, 1929) regarded all type III tails (or type $II_0$ tails, as they were referred to for some time; cf. Bobrovnikoff 1951) to be "complete" synchrones (Orlov 1960). Since outbursts occur commonly in comets, streamers are fairly frequent phenomena in their dust tails. Two outstanding examples in the past three decades are comets West (1976 VI = C/1975 V1) with at least five bright and up to seven additional streamers (Sekanina and Farrell 1978, Sekanina 1980, Akabane 1983) and comet Halley with at least six to eight streamers (Lamy 1986a, Sekanina 1986, Beisser and Boehnhardt 1987a,b). In both comets the multiple streamers were observed one to a few weeks post-perihelion and the inferred outbursts occurred within 2 weeks of the perihelion passage.

*2.3.3. Anomalous tails and antitails*

It appears that Harding (1824) and Olbers (1825) were the first to use the term *anomalous tail* in reference to a sunward-pointing extension displayed by the comet of 1823 (C/1823 Y1). The term was also employed by Olbers (1831) in what can be regarded as the first review paper on the subject. While it was suggested by Needham et al. (1957) that several records in ancient annals of the Chinese dynasties might be interpreted as referring to comets with tails on both sides of the nucleus, the first positive account of a tail in an apparent direction of the Sun was given by Kirch (1681) in his description of the comet of 1680 (C/1680 V1), calling it a pseudo tail (*After-Schwanz*).

Bredikhin's (Jaegermann 1903) hypothesis was the most ambitious one among the early efforts aimed at explaining the nature of the sunward-oriented tails, which did not fit any of the three types of his classification. Like Harding and Olbers, Bredikhin called these tails anomalous, but he distinguished two kinds: genuine and pseudo anomalous tails. Unfortunately, his results suffered from the lack of a sound physical model, from unacceptable approximations in his treatment of the problem, and from inadequate observations available. His most significant contribution to the understanding of the nature of these tails was the conclusion on their close relationship with meteor streams.

At the present time, the development of anomalous tails is fully understood. As a rule, they are made up of relatively large, often submillimeter- to millimeter-sized, particles ejected from the nucleus long (at least weeks, sometimes months or even years) before observation (e.g., Finson and Probstein 1968a, b). The basic conditions that must be satisfied for an anomalous tail to appear include two geometric constraints (e.g., Sekanina 1976): (i) the Earth must be near the comet's orbital plane and (ii) at the same time, the angle subtended, at the comet, by the comet-Earth vector and the comet's radius vector must be smaller than the lag angle $\Lambda$ of the earliest detectable dust

emission (which is always smaller than 180° at the comet), in which case the anomalous tail points toward Earth, or between 180° and 180° + Λ, in which case it points away from Earth. About the time of the Earth's transit across the comet's orbital plane, the anomalous tail becomes very sharp and is sometimes called an antitail or a sunward spike to imply that it is a thin sheet of debris confined to the orbital plane. The above geometric constraints were employed in the first successful prediction of an antitail (Sekanina 1973), which involved comet Kohoutek (1973 XII = C/1973 E1). More recent studies (e.g., Richter and Keller 1988, Fulle 1988a, b) have shown that the effect of particle ejection velocity on anomalous tails, neglected in the original Finson-Probstein (1968a) approach, ought to be accounted for in rigorous investigations and that the presence of a neckline structure (Sec. 2.3.1) further enhances the sharpness of some antitails.

Every anomalous tail, observed around the time of the Earth's transit across the orbital plane, exhibits a characteristic rotational motion about the Sun's projected direction in the sky. Invariably noticed by observers, it merely reflects the Earth's motion from one side of the comet's orbital plane to the other. The antitail's apparent rotation is clockwise at the ascending node, counterclockwise at the descending node. The antitail's sharp edge, caused by the "crowding" of pertinent synchrones, is always on the side of the radius vector: it is a leading boundary before the transit and a trailing boundary afterwards. Finally, since the lag angle of synchrones increases with their age and depends sensitively on the comet's true anomaly at the observation time, the probability of appearance of an anomalous tail increases dramatically after perihelion, especially for comets with small perihelion distances.

### *2.3.4. Striated tails and particle fragmentation*

Unlike streamers, striae are bands in the dust tail that (i) appear less commonly; (ii) are always separated from the nucleus by huge gaps; (iii) are narrow, almost perfectly rectilinear, and nearly parallel to each other; (iv) their orientations are inconsistent with those of synchronic or syndynamic formations and, when extended beyond their visible length, they intersect the radius vector almost always on the sunward side of the nucleus; and (v) tend to cluster into groups, sometimes numbering more than a dozen at a time.

The first comet in whose tail striae were positively identified (e.g., Bond 1862) was Donati (1858 VI = C/1858 L1). Early dynamical studies of striae, especially in the tail of comet 1910 I (= C/1910 A1), led to a conclusion — now known to be incorrect — that they are synchronic formations just like streamers. The most significant observed characteristic of striae was thought to be not their peculiar orientation, but the gap between their sunward end and the nucleus, which explains

why Orlov (1960) called them "terminal" synchrones to discriminate between striae and streamers.

After the appearance of another comet with striae in its tail, Mrkos (1957 V = C/1957 P1), the orientation discrepancies between striae and true synchrones could no longer be ignored. Work on this subject intensified more recently as observations of additional comets with striated tails accumulated, especially after the arrival of comet West (1976 VI = C/1975 V1). Two competing models emerged out of these efforts: Notni's (1964) high speed particle ejection theory and Sekanina and Farrell's (1980) particle fragmentation theory. Notni found that the motions of striae in the tail of comet Mrkos could be fitted on the assumption that, upon their ejection from the nucleus, dust particles interact with comet plasma so strongly that they get accelerated, in a tailward direction, to velocities of 10 km/s or more while still near the nucleus. On the other hand, Sekanina and Farrell explained the formation of striae as a two-step process: parent particles ejected in an outburst are subjected to the same, relatively high, radiation pressure acceleration during their motion through the tail, and subsequently they all fragment at the same time, at distances of up to a few million kilometers from the nucleus. For comet Mrkos, Sekanina and Farrell (1982) found two kinds of striae that consisted, respectively, of absorbing and dielectric grains (Fig. 5). Akabane (1983) employed an essentially identical approach (but a different terminology) in his investigation of comet West. Comparing the two competing models, Notni and Thänert (1988) confirmed that the fragmentation theory is consistent with the motions of striae in both Mrkos and West, but found that the high speed ejection theory fails for West. The fragmentation model was also successfully applied to comet Seki-Lines (1962 III = C/1962 C1) by Nishioka and Watanabe (1990), to comet 1910 I (= C/1910 A1) by Sekanina and Farrell (1986), and, very recently, to comet Hale-Bopp (C/1995 O1) by Pittichová et al. (1998).

Nishioka and Watanabe (1990) argued that the constraint on the fragmentation time of parent particles can fully be relaxed, if the fragments have finite lifespans (cf. also Watanabe and Nishioka 1991, Nishioka et al. 1992). However, Sekanina and Pittichová (1998) have shown that in the case of comet Hale-Bopp the condition of a constant fragmentation time can be relaxed to only a few days. The constraint on the radiation pressure acceleration of parent particles remains firm. Their source might in fact be a single massive piece so extraordinarily porous as to be optically thin, a property that could be dictated observationally by the high acceleration values. Alternatively, as shown by Fröhlich and Notni (1988), optically thick clouds of grains of a limited size spectrum could temporarily be stabilized against dissipation due to solar radiation pressure and they too could satisfy the condition of a high, constant acceleration value.

Striae are by no means the only phenomena that imply fragmentation of cometary dust. Large amounts of attogram grains, discovered by Utterback and Kissel (1990) in 1P/Halley, were interpreted by them as products of vigorous fragmentation of dust at distances of up to at least one million kilometers from the comet. Fragmentation was also invoked by Simpson et al. (1986, 1987, 1989) to explain "clusters" and "packets" of dust grains impacting the detectors onboard the Halley flyby spacecraft; by Thomas and Keller (1987) and by Keller et al. (1990) to interpret the radial brightness profiles of jets on closeup, high-resolution images returned by the Giotto's Halley Multicolour Camera and to study the hydrodynamic implications of near-nucleus dust-grain disintegration; by Combi (1994) to understand isophote dust-coma profiles on ground-based images of comets; and by Boehnhardt (1986) and Boehnhardt and Fechtig (1987), among others, to demonstrate potential effects of electrostatic dust charging in comets (Sec. 2.1.3).

## 2.4. Dust in Periodic Comet Shoemaker-Levy 9

This object, under observation from late March 1993, almost nine months after its extremely close approach to Jupiter when it had split into as many as a dozen major fragments, until it collided with Jupiter in the second half of July 1994, was one of the most observed comets ever. For many weeks and months following the initial breakup, the individual fragments continued to split in discrete events which are usually referred to as episodes of secondary fragmentation and which gave birth to the so-called off-train condensations. As argued below, continuing fragmentation was almost certainly responsible for the highly atypical size (and mass) distribution of this comet's dust population and its dynamical evolution, two issues of primary interest here.

### *2.4.1. Fragmentation model for the comet's progenitor nucleus*

At discovery the brightest part of the comet appeared as a string, or a train, of 21 discrete condensations less than 1 arcmin in length and arranged in an almost perfectly rectilinear configuration (Fig. 6). With time the separations between the condensations were gradually increasing and about one half of them began to show small but detectable deviations from the train (the so-called off-train condensations). Even though the condensations were the comet's most prominent features, significant amounts of material were also situated in between them, along the train's entire length.

The comet displayed three other kinds of morphological feature. Extending on either side of the train were the trails or wings. The west-southwestern trail was perfectly aligned with the train, whereas the east-northeastern branch appeared to be slightly inclined to it. Subtending a relatively small angle with the train and pointing almost exactly to the west was a set of parallel, rectilinear, and narrow tails,

whose roots coincided with the individual condensations in the train. These tails were immersed in, and on low-resolution images (such as the one in Fig. 6) blended with, an enormous structureless sector of material, which was stretching to the north of its sharp boundary, delineated by the nuclear train and the two trails.

The formulation of a viable model for the secondary-fragmentation events is of key importance for understanding the process of this comet's disintegration. In their comprehensive analysis, Sekanina et al. (1998) conclude that the jovian tidal forces inflicted extensive cracks throughout the interior of the progenitor nucleus but did not split it apart. The initial disruption apparently consisted of a rapid sequence of individual breakups that gave birth to 10–12 major fragments and brought about by stresses exerted on the cracked object by its fast rotation in the early post-perijove period of time. The secondary-fragmentation events are then understood as stochastic manifestations of the continuing process of progressive disintegration. The vectorial distribution of separation velocities of the secondary-fragmentation products shows a strong concentration toward a great circle, unquestionably an effect of the approximately conserved angular momentum of the progenitor comet. The velocity vectors are actually distributed within a segment of the great circle, thus implying that the subfragments were released from one side of their parents. The preferential appearance of the off-train condensations on one side of the nuclear train is thereby explained for the first time. The model requires that the points of separation be on the antisolar side of the parent fragments, where thermal stresses should enhance the effects due to the rotation stresses. The spin axis of the progenitor nucleus was situated nearly in its jovicentric orbit plane, which rules out the strengthless aggregate models (Solem 1995, Asphaug and Benz 1996) as plausible breakup scenarios. From the derived separation velocities (of up to 1.7 m/s) of the products of secondary fragmentation, the progenitor nucleus is found to have been approximately 10 km in diameter and spinning rapidly.

### *2.4.2. Dust content in the nuclear train*

The sizes and dynamics of particulate material in the individual condensations have been subject to much controversy. An internally consistent solution (cf. also Sec. 2.4.4) can be offered on the assumption that the mass distribution was dominated by the processes that occurred following its closest approach to Jupiter in July 1992.

From quantitative considerations on radiation pressure accelerations, the minimum diameter of particulates in the innermost regions of the condensations, within 0.5 arcsec (or about 1800–2000 km) of their center, is estimated at about 1 meter in late January 1994 and 2 meters some $5\frac{1}{2}$ months later, assuming a bulk density of 0.2 g/cm$^3$. The observed brightness of these innermost regions, combined with this

lower limit, makes it possible to estimate the mass involved as a function of the particles' albedo, the upper size limit, and the slope of the size distribution function. For a geometric albedo of 4%, for example, the dust cloud of the condensation $Q_1$, one of the more prominent ones, would at both times be about $1\times10^{14}$ g in mass if the size distribution varied as an inverse fourth power of the size and some $3\times10^{15}$ g, if it varied as an inverse size squared. A conservative value of 0.2 km was used to estimate the upper limit of particle diameter; the actual upper limit must in fact be greater. This mass does not include the contributions from the six fragments >1 km in diameter, detected individually in the condensation $Q_1$ on both the late January and the early July images (Sekanina 1995), which appear to have contributed collectively 8 to $9\times10^{15}$ g, assuming the same albedo and bulk density as above. Most of this mass, nearly $7\times10^{15}$ g, is found to have been concentrated in the largest fragment, which in this scenario dominated. If, on the other hand, the upper particle diameter limit in the dust cloud were near 1 km and/or the size distribution function were flatter than assumed above, the mass of the cloud would have been comparable with, or greater than, that of the largest fragment.

Relative particle velocities in the proximity of major fragments must have been extremely low, about 0.1 m/s or less, significantly lower than the separation velocities involving the events of secondary fragmentation. Indeed, the fragment $Q_2$, which split off from $Q_1$ in April 1993 with a velocity of ~0.4 m/s (Sekanina et al. 1998), appeared as a distinctly separate condensation, located far outside the $Q_1$'s dust cloud, by January 1994. Another line of evidence for very low velocities is presented in Sec. 2.4.4.

*2.4.3. The dust trails (or wings)*

Although a number of nuclear models have been presented to explain the comet's peculiar appearance, relatively little attention has been paid to the dust trails. Sekanina et al.'s (1994) model regarded the dust trails as one of manifestations of the initial disruption and the physical and dynamical conditions in the resulting cloud of debris. In particular, these authors showed that the extent and orientation of the trails can be interpreted as centimeter-sized and larger products of ubiquitous particle-particle collisions. The rotation-driven, rapidly "thermalized" particle velocity distribution of the cloud of debris was found to display a long "tail", with a small fraction of the particulates having been accelerated to velocities of up to ~7 m/s in the direction of the orbital motion, necessary to explain the maximum observed lengths of the trails. The slight inclination of the east-northeastern branch to the nuclear train can in this scenario be explained by a deficit of pebble-sized and larger particles, a possible effect due to highly irregular shape of the parent nucleus (Sekanina et al. 1994).

*2.4.4. The tails and the sector of material*

The most diagnostic information provided by the tails is their orientation as a function of time and their characteristic width, length, and appearance. The tails are perfectly parallel, which strongly suggests the same mode of their origin. The temporal variations in the orientation indicate that the release of particulates occurred most probably during the second half of 1992 (Sekanina 1996a). It is not known, however, whether the release was continuous or proceeded in a sequence of events and whether or not it was outgassing-driven. It is tempting to associate the tail formation with both the initial disription and the events of secondary fragmentation, most of which occurred in the implied time span. It is significant, however, that no tail extension was ever observed to point to the southeast of the train (cf. Fig. 6). Dust emissions from active fragments during long periods of time in 1993 and 1994 should have resulted in fairly persistent features at position angles of 100–110°. Their lack, especially on images taken with the HST, offers rather tight constraints on the dust production rate from the nuclei during some periods of time in 1993 and 1994. These upper limits are as low as 0.2 kg/s, or more than two orders of magnitude lower than the limits derived spectroscopically for the water production rate (30 to 60 kg/s; Weaver et al. 1995, corrected values) from an unsuccessful search for the hydroxyl radical.

The fact that the tails appeared as natural extensions of the condensations suggests that the particulates in both regions were of common origin and that the only major dynamical difference between them is the magnitude of solar radiation pressure acceleration to which they were subjected. This acceleration increases and therefore the characteristic particle size decreases along the tail. Particles located at a distance of about 15,000 km from the "parent" condensation on images taken shortly before the crash, were typically several centimeters in diameter. The tail width, on the other hand, is a measure of a maximum particle velocity in the plane unaffected by solar radiation pressure. The tails broadened with increasing distance from the condensation (e.g., Weaver et al. 1995), implying that smaller particles had a wider velocity distribution. From a sample of the projected linear tail widths near the nuclear train one finds upper limits on a particle velocity in a general range of 0.1 to 0.4 m/s (Sekanina 1996a), comparable with, or lower than, the separation velocities of the products of secondary fragmentation. These estimates confirm that particles in the condensations must have been larger than several centimeters in diameter and must have had velocities not exceeding about 0.1 m/s (Sec. 2.4.2).

It would be erroneous to conclude that the split comet Shoemaker-Levy 9 showed no evidence for microscopic grains, which are so abundant in other comets. Although a severe bias against such very small

particles in all observations of this comet is inherent because of the discovery some $8\frac{1}{2}$ months after the parent object's disruption, the area in the upper right corner of Fig. 6, the most remote one from the train and the trails, is populated by grains whose diameters were a few tens of microns at the most.

*2.4.5. The problem of continuing activity*

One of the most controversial issues concerning comet Shoemaker-Levy 9 is whether or not the individual fragments continued to be active. To some degree an answer to this question depends on how one defines activity. We identify activity with sublimation of ices (and parallel emission of dust) at rates that are not trivial.

The strongest arguments usually presented in favor of this comet's continuing post-breakup activity are the apparent sphericity of the condensations and a very gradual decrease in their intrinsic brightness with time (Hahn et al. 1996; Rettig and Hahn 1997; Tanigawa et al. 1996). Unquestionably, a dust cloud ejected very near Jupiter in July 1992 would soon become, and would remain, extremely elongated.

The strongest arguments against continuing activity are the failure to detect it and the already mentioned extremely low dust particle velocities as well as the implied considerable particle dimensions.

Of the two mutually exclusive scenarios, the reader can choose the one he finds less vulnerable. We note, however, that continuing spontaneous (i.e., activity-independent) fragmentation of dust in each condensation can account both for the condensation's spherically symmetric shape and for a slow rate of its brightness decrease, as argued by Tanigawa et al. (1997). Considering, on the one hand, overwhelming evidence for ubiquitous disintegration of this comet by chain fragmentation and imagining, on the other hand, the absurdity of a subdecimeter-per-second rate of expansion of a cloud of dust particles entrained in a transonic gas flow, we find the hypothesis of inactive nuclear fragments of comet Shoemaker-Levy 9 far more attractive.

Comet Shoemaker-Levy 9 strikingly illustrates the kind of extreme physical phenomena and extraordinary dynamical scenarios that one is confronted with when investigating truly exceptional cometary objects.

## 3. OPTICAL AND PHYSICAL PROPERTIES

The thermal emission and scattered radiation from the dust coma allow us to make some general statements about the optical properties, size, and composition of the dust grains.

### 3.1. Thermal Emission

The 3–20 $\mu$m thermal emission from the dust coma has been observed with infrared photometers for many comets since the first detection of

Ikeya-Seki 1965 VIII = C/1965 S1 (Becklin et al. 1966). 1P/Halley was monitored regularly in 1985–1986 (Gehrz and Ney 1992; Tokunaga et al. 1986, 1988; IHW Electronic Archive).

The observed spectral energy distribution (SED) corresponds to color temperatures $T_c$ that are 5–30% hotter than the temperature of a theoretical blackbody at the same heliocentric distance. For Halley, Tokunaga et al. (1988) find a relationship $T_c = 315.5\, r^{-0.502}$, where $r$ is the heliocentric distance in AU and $T_c$ is the 8–20 $\mu$m color temperature. The apparent color temperature is determined by the physical temperatures of the grains and their wavelength-dependent emissivities. The physical temperature of a particle in the solar radiation field depends on the balance between the solar energy absorbed at visual wavelengths and the energy radiated in the infrared:

$$\frac{\pi a^2}{r^2}\int Q_{\rm abs}(a,\lambda)\, S(\lambda)\, d\lambda = 4\pi a^2 \int \pi B(\lambda, T)\, Q_{\rm abs}(a,\lambda)\, d\lambda, \qquad (8)$$

where $S(\lambda)$ is the solar flux at 1 AU, $\pi B(\lambda, T)$ is the Planck function for grain temperature $T$, $Q_{\rm abs}(a,\lambda)$ is the absorption efficiency factor, which depends on grain size and optical constants, and $r$ is the heliocentric distance in AU.

Small carbonaceous grains absorb strongly at visual wavelengths, but cannot radiate efficiently in the infrared at wavelengths greater than about 10 times their size. Thus, they heat up until the energy radiated at 3–8 $\mu$m balances the absorbed energy. In fact, for small absorbing grains, their size controls the temperature, regardless of the specific composition (Hanner 1983). Figure 7 plots $T(r)$ for spherical glassy carbon grains. Grains smaller than about 2 $\mu$m radius are warmer than a theoretical blackbody and a grain of 0.1 $\mu$m radius can be several hundred degrees warmer than a blackbody. For these grains, $T_{\rm gr}(r) \propto r^{-0.35}$ instead of $r^{-0.5}$ expected for a blackbody. Thus, $T_{\rm gr}/T_{\rm BB}$ increases with $r$. We saw evidence of this trend in the high mid-infrared color temperatures recorded for comet Hale-Bopp at large $r$. Grains larger than a few microns will be warmer than a blackbody only if they are very fluffy and the unit structure is micron-sized or smaller (Xing and Hanner 1997).

In contrast to the small carbon grains, silicate grains radiate efficiently in the mid-infrared; it is the amount of absorption at visual wavelengths that controls their temperature. The absorption at visual wavelengths depends strongly on the iron content of the silicate (Dorschner et al. 1995). Mg-rich silicates have very low absorption (the imaginary part of the refractive index $k \sim 0.0003$ at 0.5 $\mu$m for a glass with Fe/Mg = 0.05); whereas $k \sim 0.05$ at 0.5 $\mu$m for a pyroxene glass with Fe/Mg = 1 and $k \sim 0.1$ for an olivine glass with Fe/Mg = 1. Figure 8 illustrates the dependence of temperature on $k$ for grains

of 0.5 $\mu$m radius. One sees that, for $k = 0.001$ the grain temperature is much cooler than $T_{BB}$. Setting $k = 0.01$ (Fe/Mg $\sim$ 0.5) raises the grain temperature above that of a blackbody. For Fe-rich olivine (Fe/Mg = 1; Dorschner et al. 1995), the temperature is similar to that of a fully absorbing grain; indeed, at $r < 1$ AU, the grains are hotter than a corresponding carbon grain. The temperature depends only weakly on grain size for the silicate particles. The dust mass spectra from the Halley probes indicate that the cometary silicates are Mg-rich (Jessberger et al. 1988; Lawler et al. 1989).

The cometary silicate grains must be sufficiently absorbing to be warm. Otherwise, the large amount of silicates necessary to produce a visible feature above the thermal continuum from the hot absorbing grains would result in a far stronger scattered light continuum than is observed. Either the silicates have a relatively high iron content (in contrast to the Halley results), or the grains are physically attached to absorbing material (the "mixed" particles detected during the Halley flybys).

Bradley (1994) reported that a major component of chondritic interplanetary dust particles (IDPs) consists of glass with embedded FeNi metal and sulfides (GEMS). The FeNi beads are $\sim$0.01–0.04 $\mu$m in diameter and comprise 5 to less than 10% of the volume (Bradley, private communication). For inclusions small compared to the wavelength, effective medium theory can be used to compute effective optical constants (Bohren and Huffman 1983). A volume fraction of 5% Fe beads in a Mg-rich silicate leads to an imaginary part of the refractive index $k = 0.01$, sufficient to heat the grains.

The absorptivity of organic residue grains depends on the ratio of H/C and can vary from $k \sim 0.01$ to 0.1 or more (e.g., Khare et al. 1990). Consequently, small organic grains could have temperatures ranging from $\sim T_{BB}$ up to the temperatures of small carbon grains.

We can conclude from the observed cometary SED, independent of a specific model, that the mid-infrared thermal emission arises predominantly from submicron- to micron-sized grains with strong absorption (or from very fluffy grains having structural units $\leq 1$ $\mu$m radius).

The observed color temperature corresponds to the envelope of the wavelength-dependent emission from the ensemble of grains and does not represent the physical temperature of the grains. Moreover, the color temperature can vary with wavelength, since the smallest, hottest grains will radiate more strongly at the shorter wavelengths. The comets with the strongest dust emission, such as Halley or Hale-Bopp, have higher color temperature at 3.5–8 $\mu$m than at 8–20 $\mu$m, indicating an enhanced abundance of hot submicron grains.

Although the 3–20 $\mu$m thermal emission allows us to determine the amount of small dust in the coma, these data do not help us to assess the amount of mass in large particles with their lower ratio of cross

section to mass. Thermal emission at far-infrared and submillimeter wavelengths can, in principle, constrain the abundance of large particles in the coma, since the emissivity of the smaller grains will decrease as $\lambda^{-\alpha}$, $1 \leq \alpha \leq 2$ while the emissivity of the large grains remains essentially constant.

Several comets were detected at 60 and 100 $\mu$m during the IRAS mission (Walker and Aumann 1984). The DIRBE instrument on the COBE satellite measured the spectral energy distribution from 3.5 to 100 $\mu$m for comets Okazaki-Levy-Rudenko (1989 XIX = C/1989 Q1), Austin (1990 V = C/1989 X1), and Levy (1990 XX = C/1990 K1) (Lisse et al. 1994, 1998). Only comet Levy had a color temperature $>1.10\,T_{\rm BB}$ and a drop in the average grain emissivity at 60 and 100 $\mu$m, indicating that small grains dominated the emitted radiation. This is consistent with the 10 $\mu$m spectra; among these three comets only Levy had a strong silicate feature. The photometer on the Infrared Space Observatory has also measured the long wavelength radiation from comets. Comet Hale-Bopp (C/1995 O1) was detected at $\lambda\lambda$3.6–160 $\mu$m at $2.8 < r < 4.92$ AU (Grün et al. 1998; Peschke et al. 1998).

Continuum emission at submillimeter wavelengths has been measured in several comets and can be compared with the 10 $\mu$m flux to assess the relative contributions of large and small grains. Jewitt and Luu (1990) detected emission from 23P/Brorsen-Metcalf at 800 and 1100 $\mu$m. If one compares the flux with the 10 $\mu$m flux recorded 4 days earlier, one finds that the data are consistent with a radiating blackbody having constant emissivity (Lynch et al. 1992a). That is, the large grains emitting at 800 and 1100 $\mu$m can account for the 10 $\mu$m flux as well; 23P/Brorsen-Metcalf apparently lacked the population of small grains present in most comets, consistent also with the lack of a silicate feature and the low scattered light continuum. In contrast, four other comets measured by Jewitt and Luu (1992) and Hyakutake (Jewitt and Matthews 1997) have submillimeter fluxes or upper limits that are an order of magnitude lower than the flux extrapolated from 10 $\mu$m on the assumption of constant emissivity, as summarized in Table 1. In each case, the 10 $\mu$m and submillimeter measurements were less than 14 days apart. We infer that, in these comets, the 10 $\mu$m flux arises from smaller grains which do not radiate efficiently at submillimeter wavelengths.

### 3.2. Silicates

Small silicate grains produce an emission feature near 10 $\mu$m due to stretching vibrations in Si-O bonds. The strength of this feature depends upon the grain size; grains larger than a few microns will show weak, if any, excess emission above a blackbody spectrum (Hanner et al. 1987, Rose 1979). The shape of the feature can be diagnostic of the silicate mineralogy (e.g., Hanner et al. 1994a; Stephens and Russell

1979; Hanner et al. 1998).

A 10 $\mu$m emission feature is seen in filter photometry of many new and long period comets (Ney 1974, 1982; Rieke and Lee 1974; Ney and Merrill 1976; Gehrz and Ney 1992). The feature is strongest in active comets with strong scattered light continuum at visible wavelengths. The feature was observed in comet 1P/Halley throughout the 1985–1986 apparition, from 1.3 AU preperihelion to 1.48 AU post-perihelion; the strength of the feature varied from day to day and with position in the coma, as well as with heliocentric distance (Bregman et al. 1987; Tokunaga et al. 1986, 1988; Hanner et al. 1987; Ryan and Campins 1991; Gehrz and Ney 1992).

Low resolution 8–13 $\mu$m spectra with good signal-to-noise have been acquired for about a dozen comets. Six of the comets display a strong, structured silicate emission feature. These are long-period comets Bradfield (1987 XXIX = C/1987 P1) (Hanner et al. 1990, Hanner et al. 1994a), Levy (C/1990 K1) (Lynch et al. 1992b), Hyakutake (C/1996 B2), Hale-Bopp (C/1995 O1), (Hanner et al. 1998), new comet Mueller (1994 I = C/1993 A1) (Hanner et al. 1994b), and 1P/Halley (Bregman et al. 1987; Campins and Ryan 1989).

By far the strongest emission feature is seen in comet Hale-Bopp. This comet is also unusual because strong silicate emission was already present at 4.6 AU preperihelion (Crovisier et al. 1996). The spectrum of Hale-Bopp near perihelion is presented in Fig. 9; the observed fluxes have been divided by a blackbody fitted at 8 and 12.5–13 $\mu$m. One sees that there are three peaks, at 9.2, 10, and 11.2 $\mu$m, and minor features at 11.9 and possibly 10.5 $\mu$m. The spectral shape is very similar to that in Halley (Fig. 9) and in the other comets cited above. For a review of the Hale-Bopp spectra and interpretation, see Hanner et al. (1998).

The 11.2 $\mu$m peak is attributed to crystalline olivine, based on the good spectral match with the measured spectral emissivity of Mg-rich olivine (Stephens and Russell 1979; Koike et al. 1993). Only a fraction (15–20%) of the silicate material needs to be in the form of crystalline olivine to produce the observed feature (Hanner et al. 1994a); the mass absorption coefficient of olivine near 11.3 $\mu$m is a factor of 3 to 10 times that of glassy silicates (Day 1974, 1976).

The 9.2 $\mu$m feature, first recognized in Hale-Bopp (C/1995 O1), matches that of amorphous, Mg-rich pyroxene (Stephens and Russell 1979; Dorschner et al. 1995). Amorphous or glassy olivine produces a peak at 9.8 $\mu$m (Day 1974; Stephens and Russell 1979), consistent with the interstellar silicate feature; it probably contributes to the 10 $\mu$m cometary peak. Crystalline pyroxenes generate more variety in their spectral signatures. The peaks usually occur at 10–11 $\mu$m, with a smaller peak near 9.3 $\mu$m (Sandford and Walker 1985). Wooden et al. (1998) present a spectral model including both olivine and pyroxenes, glassy and crystalline, to match the Hale-Bopp spectra. They

explain observed changes in the spectral shape with heliocentric distance by temperature differences between more transparent (cooler) Mg-rich pyroxene grains and less transparent (warmer) olivine grains.

Silicates also have a bending mode vibration at 16–24 $\mu$m; the central wavelength depends on the mineral structure. A remarkable 16–45 $\mu$m spectrum of comet Hale-Bopp (C/1995 O1) at $r = 2.9$ AU was acquired with the SWS spectrometer on the Infrared Space Observatory (Crovisier et al. 1997a), which is shown in Fig. 10. Five peaks are clearly visible, corresponding in every case to laboratory spectra of Mg-rich olivine (Koike et al. 1993). Airborne spectra of comet 1P/Halley at $r = 1.3$ AU (the only other 16–30 $\mu$m spectra of a comet) show only weak olivine features at 28.4 and 23.8 $\mu$m (Herter et al. 1987; Glaccum et al. 1987).

In summary, the spectral structure suggests a complex mineralogy for the cometary silicates, including both glassy and crystalline grains of pyroxene and olivine composition. This mineralogy is consistent with the pyroxene-rich and olivine-rich chondritic aggregate IDPs thought to originate from comets because of their porous structure, high carbon content, and relatively high atmospheric entry velocities. Thus, we can apply what has been learned in the laboratory about the chondritic aggregate IDPs to enhance our understanding of cometary dust.

The presence of Mg-rich olivine (forsterite) and Mg-rich pyroxene (enstatite) in cometary dust is significant because they are high temperature condensates. These crystalline silicates can form by direct vapor condensation at $T \sim 1400$ K followed by slow cooling or by annealing of amorphous silicates at $T \sim 900$–1000 K. The enstatite whiskers and platelets in IDPs have growth patterns that indicate direct vapor phase condensation, rather than annealing (Bradley et al. 1983). Either these grains formed in the hot inner region of the solar nebula and were transported to the region of comet formation or they were pre-existing interstellar grains present in the solar nebula.

The spectra of four other new comets discussed in Hanner et al. (1994a) are puzzling; each has a unique, and not understood, spectrum. For example, an extremely broad emission feature is present in Wilson (C/1986 P1), suggesting a very amorphous silicate material. We may be witnessing the effect of cosmic ray damage to the outermost layer of the nucleus over the lifetime of the Oort Cloud. Silicate emission was detected for the first time in two short-period comets, 4P/Faye and 19P/Borrelly (Hanner et al. 1996). The emission is broad in both comets, with no evidence for a peak at 11.2 $\mu$m. Other comets, such as 23P/Brorsen-Metcalf (Lynch et al. 1992) and many other short-period comets, lack a silicate feature; the most likely explanation is a deficiency of small grains rather than a lack of silicate material.

### 3.3. Infrared Spectral Features of Hydrocarbons

A broad emission feature centered near 3.36 $\mu$m was discovered in spectra of 1P/Halley (Combes et al. 1988; Baas et al. 1986). The emission is attributed to the stretching vibration of C–H bonds in organic molecules. A similar emission feature has been detected in every bright comet since Halley, including new, long-period, and periodic comets. The strength of the feature correlates with the water production rate, rather than with the continuum brightness, suggesting that the carrier is most likely a gas phase species (Brooke et al. 1991).

Reuter (1992) showed that methanol vibrational bands at 3.33 $\mu$m ($\nu_2$) and 3.37 $\mu$m ($\nu_9$) will contribute to the broad 3.36 $\mu$m emission. Detailed modeling of the methanol bands leads to a residual feature centered at 3.424–3.43 $\mu$m (Bockelée-Morvan et al. 1995; DiSanti et al. 1995). The strength of the residual feature correlates with water production rates and especially with the methanol abundance; thus, it is likely to arise from a gaseous species. Assuming a $g$-factor comparable to that of methanol, the abundance of the carrier is comparable to that of methanol, about 4% relative to water, making it a significant reservoir of carbon. Overtone and combination bands of methanol may also contribute. Further progress will require high spectral resolution to resolve line structure and sort out the methanol contribution.

A small, but distinct, feature at 3.29 $\mu$m is present in the spectra of the dusty comets 1P/Halley, Levy (C/1990 K1) (Davies et al. 1991) and 109P/Swift-Tuttle (DiSanti et al. 1995). In Swift-Tuttle, the feature appeared to be stronger when the dust continuum was stronger (Fig. 11). Typical of aromatic bonds, this feature could arise from polycyclic aromatic hydrocarbons either in molecules or small solid grains. An interstellar feature at 3.29 $\mu$m is associated with other bands at 6.2, 7.7, 8.6, and 11.3 $\mu$m. No evidence of the 6.2 and 7.7 $\mu$m bands is seen in 5–8 $\mu$m spectra of comets 1P/Halley (Bregman et al. 1987), Wilson (C/1986 P1) (Lynch et al. 1989), and Hale-Bopp (C/1995 O1) (Crovisier et al. 1997b).

Thus, to date, there is no positive identification of a spectral feature from CHON grains, but further study of the 3.29 $\mu$m feature is warranted.

### 3.4 Dust Scattering

The polarization, phase function, color and albedo are related to the size, composition (refractive index) and structure of the scattering particles.

To determine the scattering phase function requires observations over an extended time and heliocentric distance range as the sun-earth-comet geometry changes. Consequently, one has the problem of normalization to account for the changing dust production rate; typically, the visual continuum is normalized to the gas production rate, assuming

constant dust/gas ratio. Millis et al. (1982) derived the phase function for the dusty comet 38P/Stephan-Oterma by normalizing to the $C_2$ production rate. The phase function was a factor of two higher at phase angle $\theta$ 3–4° than at 30°, corresponding to a slope of 0.02 mag/deg. Meech and Jewitt (1987) determined a linear slope of 0.02–0.035 mag/deg for four comets observed at $0° < \theta < 25°$. They found no evidence for an opposition surge larger than 20% in 1P/Halley at $1°.37 < \theta < 8°.6$. The phase function for the comets from 0 to 30° phase is steeper than the volume scattering function of zodiacal dust derived by Lamy and Perrin (1986), but less steep than that of dark asteroids (Meech and Jewitt 1987). It is consistent with the measured phase function of fluffy absorbing particles (Hanner et al. 1981).

Only two comets, West (C/1975 V1) and Bradfield (1980 XV = C/1980 Y1), have been observed at phase angles 120°–150° (scattering angles 60°–30°) (Ney and Merrill 1976; Ney 1982). The ratio of scattered to thermal energy shows strong forward scattering. The diffraction lobe appears to be wider for the comet dust than for the zodiacal light (Lamy 1986b).

The geometric albedo of a particle is defined as the ratio of the energy scattered at 0° phase to that scattered by a white Lambert disk of the same geometric cross section (Hanner et al. 1981). Since comets are rarely observed at 0° phase, it is convenient to define $A_p(\theta)$ at phase angle $\theta$, equal to the geometric albedo times the normalized phase function. (The empirical quantity $Af\rho$ is used by A'Hearn et al. (1995) as a measure of the dust production, where $\rho$ is the field of view radius, $f$ is the filling factor, and $A$ is the albedo at the relevant phase angle; $A$ is 4 times $A_p(\theta)$.)

Hanner and Newburn (1989) summarized the $A_p(\theta)$ at J(1.25 $\mu$m) and K(2.2 $\mu$m) for several comets determined from simultaneous measurements of the scattered and thermal radiation (Fig. 12). The albedos are very low, ranging from 0.025 at large phase angle to 0.05–0.10 near 0° phase in the J bandpass. It appears that comets beyond 3 AU have higher albedo, a trend also inferred by Hartmann and Cruikshank (1984), based on the near-infrared colors.

A higher albedo for the dust during times of strong jet activity was seen in comet 1P/Halley (Tokunaga et al. 1986). This could be due to a shift in the mean grain size or to a component of less-absorbing grains ejected during outburst. Laboratory measurements of the geometric albedo for irregular absorbing particles showed a size dependence from $A_p \sim 0.08$ for particle radius 2 $\mu$m to ~0.025 for particle radius 60 $\mu$m (Giese et al. 1986).

Albedo maps of comets 21P/Giacobini-Zinner (Telesco et al. 1986), 1P/Halley (Hammel et al. 1987), and 109P/Swift-Tuttle (Fomenkova et al. 1994a) were created by combining CCD images with thermal infrared images. The albedo is not constant across the coma, indicating

variation in grain properties. In all 3 cases, the albedo increases radially from the nucleus. The lowest albedo occurs on the anti-sunward side of the nucleus in Halley and Giacobini-Zinner.

The polarization phase curve has been measured for a number of comets (Kikuchi et al. 1987; Dollfus et al. 1988; Chernova et al. 1993; Levasseur-Regourd et al. 1996). Polarization has to be observed through filters that isolate the continuum; some earlier measurements were contaminated by gas emission. All of the comets show negative polarization at small phase angles, a neutral point at $\theta_c = 21 \pm 2°$, slope $h \sim 0.2$–$0.3\%$ per deg at $\theta_c$, and maximum polarization near 90°. However, they separate into two groups having $P_{\max} \sim 10$–$15\%$ and 25%, respectively. The higher $P_{\max}$ correlates with a stronger dust continuum and stronger silicate emission feature. For particle sizes of a few tenths of a micron (size parameter ~2.5–5), silicate particles tend to have relatively low positive polarization and more negative polarization, while carbonaceous particles show stronger positive polarization (Yanamandra-Fisher and Hanner 1998); this is not consistent with the association of stronger silicate feature with higher $P_{\max}$. Only for grain radii ~0.1 $\mu$m and smaller does the maximum polarization near 90° increase for both silicate and absorbing grains. Thus, the comets in the higher $P_{\max}$ group are likely to have a higher abundance of small grains ~0.1 $\mu$m radius or fluffy aggregates of such grains. In the case of 1P/Halley, the polarization at large phase angles increased with wavelength (Dollfus et al. 1988), as one would expect if the ratio of particle size to wavelength is controlling $P_{\max}$.

Spatially resolved observations of the inner coma often show increased polarization in jets. In their study of polarization in 1P/Halley, Dollfus et al. (1988) distinguish three regions: a bright inner halo (radius $r \sim 100$ km), the inner coma or "fresh" dust ($r < 5,000$ km) and the outer coma ($r \sim 10,000$ km). The inner coma consistently produced higher polarization at large phase angles, while the halo displayed lower polarization than the other regions at $\theta = 30$–$40°$. Lower albedo near the nucleus was also apparent in Halley; both features could be consistent with an excess of larger particles surrounding the nucleus.

The color of the scattered light is generally redder than the sun; the reflectivity gradient decreases with wavelength from 5–18% per 0.1 $\mu$m at wavelengths 0.35–0.65 $\mu$m to 0–2% per 0.1 $\mu$m at 1.6–2.2 $\mu$m (Jewitt and Meech 1986). Measured near-infrared $J - H$ and $H - K$ colors are plotted in Fig. 13. The near-infrared colors of the dust may depend on heliocentric distance (Hartmann et al. 1982; Hartmann and Cruikshank 1984); however, Hanner and Newburn (1989) noted that only the $H - K$ color is less red in comets observed at $r > 3$ AU, while the $J - H$ color shows no trend with $r$. The dust is not necessarily the same color as the nucleus. In the case of 10P/Tempel 2, the $J - H$

color of the nucleus was up to 0.3 mag redder than that of the dust (Tokunaga et al. 1992).

### 3.5. Dust Size Distribution

The size distribution of the cometary dust is important for understanding the origin of the dust particles and for determining the rate of mass loss from the nucleus. A key question for the mass loss rate is whether the mass is concentrated in large or small grains.

We have discussed how the thermal spectral energy distribution (SED) depends on grain size via the size-dependent temperature and the wavelength-dependent emissivity. In principle, then, the observed SED from 5–100 $\mu$m can be used to extract the size distribution of the dust. In practice, a more modest goal is to determine the particle size range which dominates the cross section of dust in the coma. The size distribution can also be deduced from dynamical analysis of the dust tail, by comparing the brightness isophotes with computed synchrones and syndynes.

A size distribution of the form

$$n(a) = (1 - a_0/a)^M (a_0/a)^N \tag{9}$$

has been shown to give a good fit to the 5–20 $\mu$m SED of a number of comets (e.g. Hanner et al. 1985; Tokunaga et al. 1986). This form was initially applied by Sekanina and Farrell (1982) to the dynamical analysis of the dust tail of comet Mrkos (C/1957 P1). In this equation, $a_0$ is the minimum grain radius ($\sim$0.05–0.1 $\mu$m), $N$ defines the slope at large $a$, and $M$ is related to the peak grain radius, $a_p = a_0(M+N)/N$. For comets in which the color temperature is at least 10% above the blackbody temperature, $a_p$ is in the range 0.35–0.65 $\mu$m and the main contribution to the cross section comes from dust particles in the range 0.1 to 10 $\mu$m. A value of $N \sim 4.2$ has been derived for large ($a > 100\mu$m) grains observed in the antitails of several comets (e.g., Sekanina and Schuster 1978). Here, one has to distinguish between the size distribution in the coma, $n(a)$, sensed by the infrared data and the size distribution emitted from the nucleus, $Q(a)$, relevant to the dynamical analysis. These are related by the grain velocity, $Q(a) = n(a)v(a)$. Since $v(a)$ varies approximately as $a^{-0.5}$, $N = 4.2$ in the emitted size distribution corresponds to $N = 3.7$ in Eq. (9). A value of $N > 4$ means that the mass is concentrated towards the small particles.

The space probe missions to comet 1P/Halley provided an opportunity to measure directly the mass distribution in the dust coma of an active comet. The results are summarized by McDonnell et al. (1991). In particular, the Giotto DIDSY experiment covered a wide mass range, extending to millimeter grain sizes. The cumulative mass fluence is presented in Fig. 14, supplemented at $<10^{-14}$ kg by results from the PIA

experiment. The slope of 0.9 over much of the mass range is consistent with $N = 3.7$ in $n(a)$. However, the large particle mass distribution $>10^{-9}$ kg is much flatter, indicating that the total dust mass along the track sampled by Giotto was concentrated in these larger particles. If this distribution is typical of all comets, then much of the mass lost by comets is "hidden" in these larger particles and most estimates of cometary mass loss are too low. The dust production in comet Halley was very variable spatially and temporally. Giotto flew past at a time when the dust production was apparently decreasing. It is possible that the large particles were left from the earlier outburst and that the corresponding smaller, high-velocity particles had already left the inner coma.

Certainly, large particles are present in comets. Meteor streams associated with comets contain particles in this size range. Infrared-bright dust trails associated with comets were discovered by IRAS (Sykes et al. 1986, 1990); these trails consist of particles in the submillimeter size range. Radar observations of comets IRAS-Araki-Alcock (1983 VII = C/1983 H1) (Goldstein et al. 1984; Harmon et al. 1989), Hyakutake (C/1996 B2) (Harmon et al. 1997), and 1P/Halley (Campbell et al. 1989) detected the presence of large grains surrounding the nucleus. However, the submillimeter data in Table 1 would suggest that, except for 23P/Brorsen-Metcalf, the cross section is not concentrated in the largest particles in those comets.

### 3.6. Icy Grains

Given that water ice is a major component of a comet nucleus, do icy grains play an important role in the coma? A steep brightness gradient in the scattered light continuum with radial distance from the nucleus in some comets has been attributed to sublimation of icy grains and icy grains have been considered to be a source of some volatile species in the coma.

Although pure water ice grains of radius 10 $\mu$m or larger are stable against sublimation at 1 AU, the slightest admixture of absorbing material will raise their temperature into the sublimation regime (Hanner 1981). Thus, the lifetimes of even slightly dirty ice grains in a comet coma at $r < 3$ AU will be a few hours or less, limiting their range to a few hundred kilometers. Strict limits on the size and purity would be necessary to invoke sublimation of water ice grains to explain a steeper than $1/r$ brightness gradient on a scale of $10^3$–$10^4$ km (e.g., Hanner 1981). Moreover, a steep brightness gradient has also been found in thermal infrared images (Fomenkova et al. 1993) and the thermal emission certainly does not arise from icy grains. On the other hand, loss of volatiles and grain fragmentation do apparently take place in the coma. For example, an extended source of CO in comet Halley was detected by the Giotto neutral mass spectrometer (Eberhardt et al. 1987).

At heliocentric distances beyond 3 AU, retention of ice grains in the coma is more plausible. A number of new and long-period comets display a substantial coma of solid grains at $r = 4$ to 6 AU. The coma may include a significant component of water ice grains, driven off the nucleus by sublimation of a more volatile species such as CO. With their large surface area, these grains can become a significant source of water production. A'Hearn et al. (1984) proposed that the strong OH production they observed in comet Bowell (1982 I = C/1980 E1) at $r > 4$ AU was due to icy grains. In fact, the OH production rate actually decreased by an order of magnitude between $r > 4$ AU and perihelion at 3.36 AU, implying that the icy component of the grains was not being replenished. Thermal emission from the grains at $r > 4$ AU helped to constrain the temperature and total cross section of the icy grains. Hanner and Campins (1986) showed that the OH production and thermal emission were consistent only if the grains were at a temperature of ~150 K, higher than the blackbody temperature, and indicating that ice and absorbing material were well mixed.

A more direct means of establishing the existence of icy grains is to look for the infrared spectral features. Water ice has bands near 1.5, 2.2, and 3 $\mu$m; of these, the 3 $\mu$m band is the strongest. The wavelength depends upon whether one sees the feature in scattering or absorption (Hanner 1981). Broad, shallow absorption bands at 1.5 and 2.05 $\mu$m attributed to water ice were detected in the spectrum of comet Hale-Bopp (C/1995 O1) at 7 AU (Davies et al. 1997). By the time Hale-Bopp reached 4.6 AU, however, the continuum from the large coma of small warm grains was too strong to permit further detections of ice absorption bands.

An absorption feature at 2.9–3.0 $\mu$m may have been seen in comet Černis (1983 XII = C/1983 O1) at 3.3 AU (Hanner 1983). Campins et al. (1983) reported the detection of an absorption feature slightly longward of 3 $\mu$m in comet Bowell (1982 I) which they attributed to icy grains. As we have learned from 1P/Halley and subsequent comet observations, the 3 $\mu$m region in comets can be quite complex. A confirmation of the 3 $\mu$m ice feature requires a complete spectrum with modern detector arrays.

## 4. CHEMICAL AND ISOTOPIC COMPOSITION

The knowledge on cometary dust composition before the Halley missions was very limited and merely qualitative. The presence of silicates was inferred from photometric observations at 10 $\mu$m (Ney 1982) and a few metals were observed in the sun-grazing comets (Arpigny 1979). Other sources of information like meteor spectra (Yavnel 1977) or the laboratory analysis of interplanetary dust particles (IDPs; cf. chapter in this book) were too indirect, since the true cometary origin of the

material analyzed could not be established. Thus one of the most challenging goals of the three missions to comet Halley was to reveal the elemental, isotopic, and molecular composition of its dust. To that end on all missions there were almost identical impact-ionization time-of-flight mass spectrometers: PUMA-1 and PUMA-2 on the VEGA spacecraft and PIA on Giotto. The principle of their operation is described by Kissel (1986a,b). The present chapter is based on the results of these experiments, especially the results from the instrument PUMA-1 on the probe VEGA-1 that functioned best and supplied the largest volume of top-quality data. Altogether, about 5000 individual grains were measured by all three instruments. We will start with the facts that are well established from the mass spectra and then will proceed to the less secure inferences. The following aspects always have to be taken into account:

(1) The measurements were carried out at ~2 AU from Earth during the brief (about two-hour long) encounters with the coma and, obviously, cannot be repeated.

(2) The impact-ionization mass spectrometer cannot be calibrated in the laboratory since there is no technical means to accelerate analogues of micron-sized cometary particles up to 70–80 km/s, equivalent to the encounter velocity.

(3) Comprehensive theoretical description from "first principles" is unavailable (see discussions by Inogamov 1987, Jessberger et al. 1988, Lawler et al. 1989, Mukhin et al. 1991, Hornung and Kissel 1994).

(4) The total amount of analyzed cometary material was very small (about a few nanograms), probably comparable to the mass of a single IDP collected in the stratosphere (Fomenkova et al. 1992).

(5) The data provide only very indirect information on the grain structure (cf. Kissel and Krueger 1987a, Fomenkova et al. 1994b).

(6) The composition and structure of the analyzed dust grains may have been altered to some extent relative to their original state in the nucleus because of heating and UV radiation during the few hours they spent in the coma before the encounter.

### 4.1. Facts from Ion Spectra

Very early in the analysis of the mass spectra it was noted (Kissel et al. 1986a, b) that in some spectra ions of the light elements H, C, N, O show the highest intensity peaks, while other spectra are dominated by ions of the rock-forming elements like Mg, Si, Ca, and Fe. The close relationship between ions within each of these groups is demonstrated by a common factor analysis (Jessberger et al. 1988). The cometary dust particles represented by those spectra were dubbed CHON and SILICATES, respectively, where CHON denotes refractory organic material (Jessberger et al. 1986, Clark et al. 1987) and SILICATES stands for the

major rock forming elements (Jessberger et al. 1988). As will be clear from our later discussion on the mineralogic composition of Halley's dust, the term SILICATES appears to be too narrow. The presence of other compounds — such as Fe-sulfides, metal particles, etc. — suggests the term ROCK component as a more appropriate one, and it will be used throughout the paper. Lawler and Brownlee (1992) showed convincingly, however, that there is no grain consisting purely of CHON or purely of ROCK material and that even the smallest cometary particles appear to be fine scale mixtures of carbonaceous and inorganic phases, the proportion of the end member components varying from grain to grain. Fomenkova et al. (1992) proposed quantitative criteria for the classification of ion spectra. If the abundance ratio of carbon to any rock-forming element is more than 10, the particle is categorized as CHON. If this ratio is less than 0.1, the particle is included in the group ROCK; the rest are MIXED particles. According to these criteria, about a half of PUMA-1 and PUMA-2 spectra combined are MIXED, while CHON and ROCK particles each comprise about 25% of the total data set.

One of the features of the PUMA-1 and PUMA-2 instruments onboard the VEGA spacecraft (but not the PIA onboard Giotto) was the switching of the reflectron voltages every 30 seconds in order to accept ions with initial energies up to 50 eV or up to 150 eV to generate the so-called long and short spectra, respectively.

Figure 15 shows the average Mg-normalized ion abundances for a number of frequently occurring elements in both types of spectra analyzed by Langevin et al. (1987), by Jessberger et al. (1988), by Lawler et al. (1989), and by Mukhin et al. (1991). The elements H, C, and O are roughly ten times more abundant in the short spectra than in the long ones, while the relative abundances of Si, S, Ca, and Fe are about the same. Since the dust composition did not change every 30 seconds (certainly there is no hint of such a change!), the effect implies that the initial energies of CHON ions upon formation are on the average higher than those of the rock-forming ions. This finding led Kissel and Krueger (1987a) to the interpretation that cometary grains are composed of a silicate core covered by an organic refractory mantle, thus substantiating pre-Halley hypotheses (Greenberg 1982).

Analysis of the spatial distributions of the various types of particles in the coma based on the PUMA-1 data (Fomenkova et al. 1994b) established that ROCK particles (depleted in organic material) dominate the outer regions of the coma, while CHON and mixed particles are relatively more abundant closer to the nucleus. This observation indicates that the less refractory fraction of the organic component is lost from the grains as they spend some time in the coma. Partial volatilization of organics releases smaller ROCK grains further out from the nucleus, while providing the extended source for CO, $H_2CO$, CN, and some other

species in the gas coma (Eberhardt et al. 1987, A'Hearn et al. 1986). This interpretation suggests that cometary grains have an "IDP-type" structure: a carbonaceous matrix with tiny silicate granules embedded rather than the core-mantle structure mentioned above. Both ideas can be reconciled by considering the possible size dependence of the grain structure: the core-mantle type for small grains, the IDP type for larger ones.

Mass spectrometric analysis itself yields information on the isotopic composition of the studied elements. However, because the signal-to-noise ratio was not high enough, isotopic information was obtained only for a few among the most abundant elements in the mass spectra of the grains: C, Mg, Si, S, Cl (terrestrial contaminator), and Fe. The isotopic ratios are generally normal, i.e., within large uncertainties they are indistinguishable from the terrestrial values (Solc et al. 1986, 1987, Sagdeev et al. 1987, Grün and Jessberger 1990, Fomenkova et al. 1992). Specifically, a $^{26}$Mg excess — from the now extinct $^{26}$Al — larger than a factor of two is excluded (Jessberger et al. 1989). The $^{12}$C/$^{13}$C ratios below the normal value — as encountered in meteoritic stardust — are inaccessible for the PIA and PUMA instruments because of unavoidable molecular interferences. A clear indication of an isotopic anomaly has been found only for light carbon (Jessberger and Kissel 1991): a few $^{12}$C/$^{13}$C ratios are much higher than the normal value of 89 and range up to 5000. Graphite grains exhibiting similarly high ratios were extracted from the carbonaceous chondrite Murchison meteorite (Zinner et al. 1990). Ultralight carbon can be produced in He-burning or explosive H-burning processes and, thus, is indicative of a circumstellar origin of those grains (Anders and Zinner 1993). Therefore, Fomenkova and Chang (1996) hypothesized that cometary dust may contain a certain fraction of circumstellar solids, in addition to refractory interstellar materials. The particle with the isotopically lightest carbon, i.e., with the highest $^{12}$C/$^{13}$C ratio in the PUMA-1 data, is composed of almost pure $^{12}$C (99 wt%) and, in addition, contains 0.5 wt% by weight of rocky material which most probably consists of FeS and Fe-poor pyroxene with a trace of FeNi. This is a typical C-grain (Fomenkova et al. 1994b; see below).

There are a few other features of the dust particles that were further deduced from the mass spectra. From the number of projectile (cometary) ions and target (silver) ions the densities and masses of the projectiles have been estimated (Maas et al. 1989). CHON-dominated particles on the average are less dense ($\sim$1 g/cm$^3$) than the ROCK-dominated particles ($\sim$2–3 g/cm$^3$), the masses of individual dust grains being from $10^{-16}$ to $10^{-11}$ g. The dust particle masses were also estimated from the so-called front end channel signals (Fomenkova et al. 1991). These are electrical signals from the target, the accelerating grid, the photomultiplier, and the catcher grid that were measured dur-

ing the collision of a dust particle with the target of the instrument and stored with the resulting mass spectrum. The mass of cometary particles was found to be comparable to that deduced by Maas et al. (1989): $5 \times 10^{-17}$ to $5 \times 10^{-12}$ g. For the density of the order of 0.3–3 g/cm$^3$ the radii of the cometary particles in question would be 0.2–2 $\mu$m.

With all the uncertainties involved in the dust particle mass determination, all authors agree that the analyzed grains were very small: the total mass of the cometary solid matter investigated by the PUMA and PIA instruments was only a few nanograms. Fortunately, the measured particles were not collected from one spot, but originated from different parts of the nucleus, thereby providing a somewhat representative sample of the comet. Note, however, that the proper comparison of the composition and properties of the measured Halley particles with those of IDPs and meteorites can be made only if these extraterrestrial materials are also sampled on the same sub-micron scale.

Three attempts have been made to gain more insight into the nature of the refractory organic component, CHON. Clark et al. (1987) qualitatively identified different types of particles based on the presence of the various combinations of H, C, O, N ions (i.e., [H,C], [H,C,N], etc.) in the spectra measured by the PIA onboard the Giotto spacecraft. The quantitative analysis, however, was hampered by the malfunction of this instrument's amplifier during the encounter.

Kissel and Krueger (1987a) considered 43 spectra of PUMA-1 and analyzed the residuals that remained after the peaks due to the obvious atomic ions had been removed from the spectra. Some of the residual peaks were identified with complex molecular ions and a number of organic-substance classes was therefore inferred to be present in cometary dust. However, an alternative explanation of these peaks in the mass spectra was later suggested by a number of authors (Sagdeev et al. 1989, Utterback and Kissel 1990). They showed that the peaks were (i) statistically random, (ii) caused by impacts of very small, attogram grains present in the P/Halley's coma very far, almost one million kilometers, from the nucleus.

Finally, Fomenkova et al. (1994b) applied cluster analysis to 515 PUMA-1 and PUMA-2 spectra dominated by CHON ions. They detected more than 30 distinguishable types of grains. The majority of Halley's organic particles appears to be multicomponent mixtures of carbon phases and organic compounds. In most cases, the available data do not warrant an unambiguous identification of corresponding compound types, but some general conclusions about the makeup of cometary nonvolatile organics still can be made. For example, elemental carbon grains composed essentially of carbon with other elements at the level of ~1% (C-grains) have been found in cometary dust and they contain ~8–10% of the total solid carbon in Halley. Note that current models for interstellar dust estimate that up to 50% of the solid carbon

in the interstellar medium is locked up in graphite or amorphous carbon (Tielens and Allamandola 1987), while in carbonaceous chondrites well characterized carbon phases occur in rather low abundances of ~2% (Zinner et al. 1990).

Other compositionally simple candidates for components of cometary solid organics are aliphatic and aromatic hydrocarbons (PAHs), and polymers of carbon suboxide ($C_nCO$) and of cyanopolyynes ($HC_nN$ or $NC_nN$). Cometary dust also appears to contain heteropolymers and/or variable mixtures of various alcohols, aldehydes, ketones, acids and amino acids, and their salts. The simplest members of those homologous series occur in the interstellar medium (Irvine and Knacke 1989). However, the molecular weight of the cometary compounds should be high enough to prevent them from evaporation since the grains in the coma may reach a temperature of a few hundred Kelvin. A variety of similarly nonvolatile compounds were found in the Murchison meteorite (Cronin and Chang 1993). These meteoritic organics often carry deuterium enrichments indicative of their interstellar origin. Finally, a similar set of products — polyalcohols, ethers, esters, carboxylic acids, and hydrocarbons — was observed in laboratory experiments where organic residues ("cometary ice tholins") were produced by plasma discharge irradiation of water/methanol/carbon dioxide/ethane cocondensed ices (McDonald et al. 1996). These experiments were intended to model the production of complex organics from simple interstellar ices which is considered as one of the possible mechanisms for formation of cometary organics.

We conclude that the compositional variety of types of cometary organic compounds is consistent with the interstellar dust model of comets (Greenberg 1982) and probably reflects the original diversity in the population of interstellar grains and/or the differences in the evolutionary history of precursor dust. Hopefully, the Rosetta mission will test some of those findings and shed more light on the nature of cometary organics.

### 4.2. Bulk Composition

Unknown yields of elements ionized by a hypervelocity impact present a problem when calculating bulk elemental abundances from ion abundances registered in the mass spectra. As we stated in the beginning of this Section, straightforward quantitative pre-flight calibrations of the instruments in the laboratory were not possible. Therefore, several empirical and theoretical approaches to the problem of conversion of the spectra from ions into atoms have been explored by various authors. Lawler et al. (1989) suggested empirical correction factors that place the peaks of the histograms of corrected Mg/Si, Fe/Si, and Fe/Mg ratios at the proper solar ratios. Jessberger et al. (1988) used yields calculated by Kissel and Krueger (1987b) from the results of experiments

with dust particles accelerated up to 40 km/s, ion yields obtained by SIMS methods, and theoretical considerations. The fact that the derived total bulk atom abundances were solar within a factor of less than 2, has been used as a justification for the proposed coefficients. Mukhin et al. (1991), however, showed that if the bulk ion abundances of rock-forming elements in comet Halley dust are calculated without correction factors, but with the mass of dust particles taken into account (i.e., the contribution of each particle to the bulk abundances is proportional to its mass), then the resulting abundances are similarly close to the solar values.

Obvious shortcomings of all these approaches are that (i) none of them considers a possible dependence of ion yields on the mass of a colliding dust particle (that is, on the total number of ions in the post-impact plasma cloud); (ii) possible matrix effects (that is, the collective effects produced by ions of various elements upon each other) are neglected. Recently, a new attempt has been made to model "from first principles" the processes within an expanding plasma cloud under the conditions corresponding to those of the PUMA/PIA measurements (Hornung and Kissel 1994). When completed, these results may lead to a better understanding of the physics of the hypervelocity impact and facilitate further interpretations of the PUMA/PIA results.

For now, the firm conclusion of all studies is that the bulk abundances of the major rock-forming elements integrated over all spectra are solar (that is, indistiguishable CI-chondritic — Anders and Grevesse 1989) within a factor of $<2$, which characterizes the overall accuracy of measurements. The average solar/chondritic elemental abundances substantiate the view that comet Halley accreted from the same nebular reservoir as the rest of the solar system, while the wide diversity in individual grain composition underscores the unequilibrated nature of comet Halley material.

All studies of Halley's dust have found that, in contrast to the rock forming elements, the CHON elements H, C, and N are enriched relative to their CI-chondritic abundances; some studies have found that O is as well. The depletion of these "non-condensible" elements in CI-chondrites relative to the Sun is interpreted as early loss of these elements. Thus, the lesser depletion of H, C, and N in cometary dust testifies that cometary solids are more primitive than CI-chondrites.

Grün and Jessberger (1990) suggested that the abundance of volatile elements in the whole comet, i.e., dust + ice (the latter measured as the gas; Krankowsky and Eberhardt 1990), is solar. From fitting both the C and O abundances to solar, they derived a cosmochemical dust/gas mass ratio of two in excellent agreement with an independent physical dust/gas ratio determination of 2.2 (Hughes 1988). Hydrogen and nitrogen were shown to be depleted in the dust + ice relative to solar by factors of 600 and 2, respectively (Grün and Jessberger 1990,

Fomenkova and Chang 1996). An earlier estimate (Geiss 1987) showing the depletion of N by a factor of 3 was based on too low a dust/gas ratio of 0.5. For the improved estimate of the dust-to-gas ratio of 2.2 : 1 (Hughes 1988), the partition of the volatile elements between gas and dust is 1 : 2 for C and N, and 2 : 1 for H and O. Apparently, C and N occur predominantly in cometary dust, while H and O prevail in the gas phase, as expected for a water-rich object (Fomenkova and Chang 1996).

### 4.3. Mineralogical Composition

To infer information on the mineralogic composition of the dust grains, one needs to know exact yields — which convert ions to atoms — with uncertainty much smaller than a factor of two. Since they are not available, a number of approaches as described in Jessberger et al. (1988), Jessberger and Kissel (1991), Fomenkova et al. (1992) and references therein were undertaken to circumvent the problem. Although these approaches cannot do without circular reasoning, they all basically show that Halley's grains are not in chemical equilibrium. This is demonstrated by the broad distribution of Fe/(Fe + Mg) ratios (Brownlee et al. 1987; Jessberger et al. 1988, 1989; Lawler et al. 1989) and also by comparison of the Mg-Si-Fe distributions of Halley's grains (Jessberger and Kissel 1991, Jessberger 1993) with that of anhydrous and hydrated interplanetary dust particles and meteorites (Bradley et al. 1989, Germani et al. 1990).

Rietmeijer et al. (1989) inferred the presence of hydrated silicates from the PUMA-2 data and Fomenkova et al. (1992) identified Mg-carbonate particles in cometary dust. These minerals are abundant in CI and CM meteorites where they formed as a result of aqueous activity on the parent bodies. Therefore, their presence in comet Halley indicates the possibility of hydration in the history of cometary dust. The hydration of cometary material could not have taken place in the nebula (Prinn and Fegley 1989), but probably occurred *in situ* in the hydrocryogenic mode. Note that carbonates and layer silicates are minor but persistent phases in anhydrous chondritic porous IDPs as well.

Fomenkova et al. (1992) also analyzed Fe-rich particles and found metal, iron oxide, iron sulfides, Fe-rich sililcates, and mixtures of these minerals in Halley's grains. Some of these grains are Ni-poor and some are Ni-rich, the mean ratio of Ni/Fe being $0.14 \pm 0.03$.

Finally, the absence of Ca-Al-rich grains (the earliest objects formed in the solar system) at least in the analyzed portion of the spectra has been demonstrated by Jessberger et al. (1989). Fomenkova and Chang (1994) have discussed the absence of SiC grains (an interstellar compound found in meteorites) in the PUMA data and estimated the upper limit of SiC in cometary dust as <150 ppm (to compare with

6–8 ppm in meteorites; Anders and Zinner 1993).

In the most recent study of Halley's dust, Schulze et al. (1996) found the mineralogical composition shown in Table 2.

### 4.4. Conclusion

The PIA/PUMA experiments onboard the Giotto and VEGA missions to comet Halley for the first time provided information on the chemical composition and nature as well as on the isotopic composition of cometary dust. Despite limitations and uncertainties, they brought about a quantum jump compared to what had been known before the missions. They also prepared the baseline for the two next approved cometary missions, ROSETTA and STARDUST, that are expected to yield data with a higher degree of security and much more details. Moreover, only the laboratory and *in-situ* analysis of dust from two more comets will address the issue of the singularity or normality of Halley's comet.

## ACKNOWLEDGEMENTS

This research was carried out in part at the Jet Propulsion Laboratory, California Institute of Technology, under contract with the National Aeronautics and Space Administration.

## REFERENCES

A'Hearn, M. F., Hoban, S., Birch, P. V., Bowers, C., Martin, R., and Klinglesmith. D. A. 1986. CN jets in comet P/Halley. *Nature* 324:649–651.

A'Hearn, M. F., Millis, R. L., Schleicher, D. G., Osip, D. J., and Birch, P. V. 1995. The ensemble properties of comets: Results from narrowband photometry of 85 comets, 1976-1992. *Icarus* 118:223-270.

A'Hearn, M. F., and Schleicher, D. G. 1988. Comet P/Encke's nongravitational force. *Astrophys. J.* 331:L47–L51.

A'Hearn M. F., Schleicher, D. G., Feldman, P. D., Millis, R. L. and Thompson, D. T. 1984. Comet Bowell 1980b. *Astron. J.* 89:579–591.

Akabane, T. 1983. The secondary tail of comet 1976 VI West. *Publ. Astron. Soc. Japan* 35:565–578.

Anders, E., and Grevesse, N. 1989. Abundances of the elements: Meteoritic and solar. *Geochim. Cosmochim. Acta* 53:197–214.

Anders, E., and Zinner, E. 1993. Interstellar grains in primitive meteorites: diamond, silicon carbide, and graphite. *Meteoritics* 28:490–514.

Arpigny, C. 1979. Relative abundances of the heavy elements in comet Ikeya-Seki (1965 VIII). In *Les éléments et leurs isotopes dans l'univers*, XXII$^{e}$ Coll. Int. d'Astrophys. (Liège: Université de Liège), pp. 189–197.

Arrhenius, S. A. 1900. Ueber die Ursache der Nordlichter. *Phys. Zeitschr.* 2:81–110.

Asphaug, E., and Benz, W. 1996. Size, density, and structure of comet Shoemaker-Levy 9 inferred from the physics of tidal breakup. *Icarus* 121:225–248.

Baas, F., Geballe, T. R., and Walther, D. M. 1986. Spectroscopy of the 3.4 micron emission feature in comet Halley. *Astrophys. J.* 311:L97–L101.

Becklin, E. E., and Westphal, J. A. 1966. Infrared observations of comet 1965f. *Astrophys. J.* 145:445-453.

Beisser, K., and Boehnhardt, H. 1987a. Evidence for the nucleus rotation in streamer patterns of comet Halley's dust tail. *Astrophys. Space Sci.* 139:5–12.

Beisser, K., and Boehnhardt, H. 1987b. Dust tail streamers and Halley's nucleus rotation. In *Diversity and Similarity of Comets*, ESA SP-278, eds. E. J. Rolfe and B. Battrick (Noordwijk: ESTEC), pp. 665–670.

Bessel, F. W. 1836. Beobachtungen ueber die physische Beschaffenheit des Halley'schen Kometen und dadurch veranlasste Bemerkungen. *Astron. Nachr.* 13:185–232.

Bobrovnikoff, N. T. 1951. Comets. In *Astrophysics*, ed. J. A. Hynek (New York: McGraw-Hill), pp. 302–356.

Bockelée-Morvan, D., Brooke, T. Y., and Crovisier, J. 1995. On the origin of the 3.2- to 3.6-$\mu$m emission features in comets. *Icarus* 116:18–39.

Bockelée-Morvan, D., and Gérard, E. 1984. Radio observations of the hydroxyl radical in comets with high spectral resolution. Kinematics and asymmetries of the OH coma in C/Meier (1978 XXI), C/Bradfield (1979 X), and C/Austin (1982g). *Astron. Astrophys.* 131:111–122.

Boehnhardt, H. 1986. The charge of fluffy dust grains of silicate and carbon near P/Halley and P/Giacobini-Zinner. In *Exploration of Halley's Comet*, ESA SP-250, eds. B. Battrick, E. J. Rolfe, and R. Reinhard (Noordwijk: ESTEC), Vol. 2, pp. 207–213.

Boehnhardt, H., and Fechtig, H. 1987. Electrostatic charging and fragmentation of dust near P/Giacobini-Zinner and P/Halley. *Astron. Astrophys.* 187:824–828.

Bohren, C. F., and Huffman, D. R. 1983. *Absorption and Scattering of Light by Small Particles.* (New York: Wiley.)

Bond, G. P. 1862. Account of the great comet of 1858. *Ann. Harvard Coll. Obs.* 3:1–372.

Bradley, J. P. 1994. Chemically anomalous, preaccretionally irradiated grains in interplanetary dust from comets. *Science* 265:925–929.

Bradley, J. P., Brownlee, D. E., and Veblen, D. R. 1983. Pyroxene whiskers and platelets in interplanetary dust: evidence of vapour phase growth. *Nature* 301:473–477.

Bradley, J. P., Germani, M., and Brownlee, D. 1989. Automated thin-film analyses of anhydrous interplanetary dust particles in the analytical electron microscope. *Earth Planet. Sci. Lett.* 93:1-13.

Bregman, J. D., Campins, H., Witteborn, F. C., Wooden, D. H., Rank, D. M., Allamandola, L. J., Cohen, M., and Tielens, A.G.G.M. 1987. Airborne and groundbased spectrophotometry of comet P/Halley from 5–13 micrometers. *Astron. Astrophys.* 187:616–620.

Brooke, T. Y., Tokunaga, A. T., and Knacke, R. F. 1991. Detection of the 3.4 $\mu$m emission feature in comets P/Brorsen-Metcalf, and Okazaki-Levy-Rudenko (1989r) and an observational summary. *Astron. J.* 101:268–278.

Brownlee, D., Wheelock, M., Temple, S., Bradley, J., and Kissel, J. 1987. A quantitative comparison of comet Halley and carbonaceous chondrites at the submicron level. *Lunar Planet. Sci. Conf.* 18:133–134.

Burns, J. A., Lamy, P. L., and Soter, S. 1979. Radiation forces on small particles in the solar system. *Icarus* 40:1–48.

Campbell, D. B., Harmon, J. K., and Shapiro, I. I. 1989. Radar observations of comet Halley. *Astrophys. J.* 338:1094–1105.

Campins, H., Rieke, G. H., and Lebofsky, M. J. 1983. Ice in comet Bowell. *Nature* 302:405-406.

Campins, H., and Ryan, E. V. 1989. The identification of crystalline olivine in cometary silicates. *Astrophys. J.* 341:1059–1066.

Chernova, G. P., Kiselev, N. N., and Jockers, K. 1993. Polarimetric characteristics of dust particles as observed in 13 comets: Comparisons with asteroids. *Icarus* 103:144–158.

Clark, B., Mason, L., and Kissel, J. 1987. Systematics of the "CHON" and other light-element particle populations in comet P/Halley. *Astron. Astrophys.* 187:779–784.

Combes, M., Moroz, V. I., Crovisier, J., Encrenaz, T., Bibring, J-.P., Grigoriev, A. V., Sanko, N. F., Coron, N., Crifo, J. F., Gispert, R., Bockelée-Morvan, D., Nikolsky, Yu. V., Krasnopolsky, V. A., Owen, T., Emerich, C., Lamarre, J. M., and Rocard, F. 1988. The 2.5–12-$\mu$m spectrum of comet Halley from the IKS-VEGA experiment. *Icarus* 76:404–436.

Combi, M. R. 1994. The fragmentation of dust in the innermost comae of comets: possible evidence from groun-based images. *Astron. J.* 108:304–312.

Cremonese, G., and Fulle, M. 1989. Photometrical analysis of the neckline structure of comet Halley. *Icarus* 80:267-279.

Cremonese, G., and Fulle, M. 1990. The dust tail of comet Wilson 1987 VII. *Astron. J.* 100:1285–1292.

Crifo, J. F. 1991. Hydrodynamic models of the collisional coma. In *Comets in the Post-Halley Era*, eds. R. L. Newburn, Jr., M. Neugebauer, and J. Rahe (Dordrecht: Kluwer), pp. 937–989.

Cronin, J., and Chang, S. 1993. Organic matter in meteorites: molecular and isotopic analysis of the Murchison meteorite. In *The Chemistry of Life's Origin*, eds. J. M. Greenberg, C. X. Mendoza-Gomez, and V. Pirronello (Dordrecht: Kluwer), pp. 209–258.

Crovisier, J., Brooke, T. Y., Hanner, M. S., Keller, H. U., Lamy, P. L., Altieri, B., Bockelée-Morvan, D., Jorda, L., Leech, K., and Lellouch, E. 1996. The infrared spectrum of comet C/1995 O1 (Hale-Bopp) at 4.6 AU from the Sun. *Astron. Astrophys.* 315:L385–L388.

Crovisier, J., Leech, K., Bockelée-Morvan, D., Brooke, T. Y., Hanner, M. S., Altieri, B., Keller, H. U., and Lellouch, E. 1997a. The spectrum of comet Hale-Bopp (C/1995 O1) observed with the Infrared Space Observatory at 2.9 astronomical units from the sun. *Science* 275:1904-1907.

Crovisier, J., Leech, K., Bockelée-Morvan, D., Brooke, T. Y., Hanner, M. S., Altieri, B., Keller, H. U., and Lellouch, E. 1997b. The infrared spectrum of comet Hale-Bopp. In *First ISO Workshop on Analytical Spectroscopy*, ESA SP-419, eds. A. M. Heras, K. Leech, N. R. Trams, and M. Perry (Noordwijk: ESTEC), pp. 137–140.

Davies, J. K., Green, S. F., and Geballe, T. R. 1991. The detection of a strong 3.28 $\mu$m emission feature in comet Levy. *Mon. Not. R. Astron. Soc.* 251:148–151.

Davies, J. K., Roush, T. L., Cruikshank, D. P., Bartholomew, M. J., Geballe, T. R., Owen, T., and de Bergh, C. 1997. The detection of water ice in comet Hale-Bopp. *Icarus* 127:238–245.

Day, K. L. 1974. A possible identification of the 10-micron "silicate" feature. *Astrophys. J.* 192:L15–L17.

Day, K. L. 1976. Further measurements of amorphous silicates. *Astrophys. J.* 210:614–617.

de Pater, I., Palmer, P., Snyder, L. E., and Ip, W.-H. 1986. VLA observations of comet Halley: The brightness distribution of OH around the comet. In *Exploration of Halley's Comet*, ESA SP-250, eds. B. Battrick, E. J. Rolfe, and R. Reinhard (Noordwijk: ESTEC), Vol. 1, pp. 409–412.

DiSanti, M. A., Mumma, M. J., Geballe, T. R., and Davies, J. K. 1995. Systematic observations of methanol and other organics in comet P/Swift-Tuttle: discovery of new spectral structure at 3.42 $\mu$m. *Icarus* 116:1–17.

Dollfus, A., Bastien, P., Le Borgne, J.-F. Levasseur-Regourd, A. C., and Mukai, T. 1988. Optical polarimetry of P/Halley: synthesis of

the measurements in the continuum. *Astron. Astrophys.* 206:348–356.

Dorschner, J., Begemann, B., Henning, Th., Jager, C., and Mutschke, H. 1995. Steps toward interstellar silicate mineralogy II. Study of Mg-Fe silicate glasses of variable composition. *Astron. Astrophys.* 300:503–520.

Dorschner, J., Friedemann, C. Gürtler, J., and Henning, T. 1988. Optical properties of glassy bronzite and the interstellar silicate bands. *Astron. Astrophys.* 198:223–232.

Eberhardt, P., Krankowsky, D., Schulte, W., Dolder, U., Lämmerzahl, P., Berthelier, J. J., Woweries, J., Stubbemann, U., Hodges, R. R., Hoffman, J. H., and Illiano, J. M. 1987. The CO and $N_2$ abundance in comet P/Halley. *Astron. Astrophys.* 187:481–484.

Finson, M. L., and Probstein, R. F. 1968a. A theory of dust comets. I. Model and equations. *Astrophys. J.* 154:327–352.

Finson, M. L., and Probstein, R. F. 1968b. A theory of dust comets. II. Results for Comet Arend-Roland. *Astrophys. J.* 154:353–380.

Fomenkova, M. N., and Chang, S. 1994. Carbon in comet Halley dust particles. In *Analysis of Interplanetary Dust*, eds. M. E. Zolensky, T. L. Wilson, F. J. M. Rietmeijer, and G. J. Flynn (American Institute of Physics), pp. 193–202.

Fomenkova, M. N., and Chang, S. 1996. The link between cometary and interstellar dust. In *The Cosmic Dust Connection*, ed. J. M. Greenberg (Dordrecht: Kluwer), pp. 459–465.

Fomrnkova, M., Larson, S., Jones, B., and Pina, R. 1994a. Albedo maps of comet Swift-Tuttle. *Bull. Am. Astron. Soc.* 26:1119.

Fomenkova, M. N., Chang, S., and Mukhin, L. M. 1994b. Carbonaceous components in the comet Halley dust. *Geochim. Cosmochim. Acta* 58:4503–4512.

Fomenkova, M. N., Evlanov, E. N., Mukhin, L. M., and Prilutskii, O. F. 1991. Determination of mass of comet Halley dust particles. *Lunar Planet. Sci. Conf.* 22:397–398.

Fomenkova, M. N., Jones, B., Pina, R. K., Puetter, R. C., McFadden, L. A., Abney, F., and Gehrz, R. D. 1993. Thermal-infrared high-resolution imaging of comet Austin. *Icarus* 106:489–498.

Fomenkova, M. N., Kerridge, J., Marti, K., and McFadden, L. 1992. Compositional trends in rock-forming elements of comet Halley dust. *Science* 258:266–269.

Fröhlich, H.-E., and Notni, P. 1988. Radiation pressure — a stabilizing agent of dust clouds in comets? *Astron. Nachr.* 309:147–155.

Fulle, M. 1987a. A new approach to the Finson-Probstein method of interpreting cometary dust tails. *Astron. Astrophys.* 171:327–335.

Fulle, M. 1987b. A possible neck-line structure in the dust tail of comet Halley. *Astron. Astrophys.* 181:L13–L14.

Fulle, M. 1987c. Meteoroids from comet Bennett 1970 II. *Astron. As-*

*trophys.* 183:392–396.

Fulle, M. 1988a. Meteoroids from comets Arend-Roland 1957 III and Seki-Lines 1962 III. *Astron. Astrophys.* 189:281–291.

Fulle, M. 1988b. Meteoroids from comet Kohoutek 1973 XII. *Astron. Astrophys.* 201:161–168.

Fulle, M. 1989. Evaluation of cometary dust parameters from numerical simulations: comparison with an analytical approach and the role of anisotropic emissions. *Astron. Astrophys.* 217:283–297.

Fulle, M. 1992. A dust-tail model based on Maxwellian velocity distribution. *Astron. Astrophys.* 265:817–824.

Fulle, M., Barbieri, C., and Cremonese, G. 1987. The dust tail of comet Halley. In *Diversity and Similarity of Comets*, ESA SP-278, eds. E. J. Rolfe and B. Battrick (Noordwijk: ESTEC), pp. 639–644.

Fulle, M., Barbieri, C., and Cremonese, G. 1988. The dust tail of comet P/Halley from ground-based CCD images. *Astron. Astrophys.* 201:362–372.

Fulle, M., Böhm, C., Mengoli, G., Muzzi, F., Orlandi, S., and Sette, G. 1994. Current meteor population of comet P/Swift-Tuttle 1992t. *Astron. Astrophys.* 292:304–310.

Fulle, M., Bosio, S., Cremonese, G., Cristaldi, S., Liller, W., and Pansecchi, L. 1993a. The dust environment of comet Austin 1990 V. *Astron. Astrophys.* 272:634–650.

Fulle, M., Cremonese, G., Jockers, K., and Rauer, H. 1992. The dust tail of comet Liller 1988 V. *Astron. Astrophys.* 253:615–624.

Fulle, M., Mennella, V., Rotundi, A., Colangeli, L., Bussoletti, E., and Pasian, F. 1993b. The dust environment of comet P/Grigg-Skjellerup as evidenced from ground-based observations. *Astron. Astrophys.* 276:582–588.

Fulle, M., and Sedmak, G. 1988. Photometrical analysis of the neck-line structure of comet Bennett 1970 II. *Icarus* 74:383–398.

Gehrz, R. D., and Ney, E. P. 1992. 0.7–23 $\mu$m photometric observations of P/Halley 1986 III and six recent bright comets. *Icarus* 100:162–186.

Geiss, J. 1987. Composition measurements and the history of cometary matter. *Astron. Astrophys.* 187:859–866.

Germani, M., Bradley, J. P., and Brownlee, D. 1990. Automated thin-film analyses of hydrated interplanetary dust particles in the analytical electron microscope. *Earth Planet. Sci. Lett.* 101:162–179.

Giese, R. H., Killinger, R. T., Kneissel, B., and Zerull, R. H. 1986. Albedo and color of dust grains: Laboratory versus cometary results. In *Exploration of Halley's Comet*, ESA SP-250, eds. B. Battrick, E. J. Rolfe, and R. Reinhard (Noordwijk: ESTEC), Vol. 2, pp. 53–57.

Glaccum, W., Moseley, S. H., Campins, H., and Lowenstein, R. F. 1987. Airborne spectrophotometry of P/Halley from 20 to 65 microns.

*Astron. Astrophys.* 187:635–638.

Goldstein, R. M., Jurgens, R. F., and Sekanina, Z. 1984. A radar study of comet IRAS-Araki-Alcock 1983d. *Astron. J.* 89:1745–1754.

Gombosi, T. I. 1986. A heuristic model of the comet Halley dust size distribution. In *Exploration of Halley's Comet*, ESA SP-250, eds. B. Battrick, E. J. Rolfe, and R. Reinhard (Noordwijk: ESTEC), Vol. 2, pp. 167–171.

Gombosi, T. I. 1991. Multidimensional dusty gasdynamical models of inner cometary atmospheres. In *Comets in the Post-Halley Era*, eds. R. L. Newburn, Jr., M. Neugebauer, and J. Rahe (Dordrecht: Kluwer), pp. 991–1001.

Gombosi, T. I., Cravens, T. E., and Nagy, A. F. 1985. Time-dependent dusty gas dynamical flow near cometary nuclei. *Astrophys. J.* 293:328–341.

Gombosi, T. I., Szegö, K., Gribov, B. E., Sagdeev, R. Z., Shapiro, V. D., Shevchenko, V. I., and Cravens, T. E. 1983. Gas dynamic calculations of dust terminal velocities with realistic dust size distributions. In *Cometary Exploration*, ed. T. I. Gombosi (Budapest: Hungarian Academy of Sciences), Vol. 2, pp. 99–111.

Greenberg, J. M. 1982. What are comets made of? A model based on interstellar dust. In *Comets*, ed. L. L. Wilkening (Tucson: University of Arizona), pp. 131–163.

Greenberg, J. M., Mizutani, H., and Yamamoto, T. 1995. A new derivation of the tensile strength of cometary nuclei: application to comet Shoemaker-Levy 9. *Astron. Astrophys.* 295:L35–L38.

Grün, E., and Jessberger, E. K. 1990. Dust. In *Physics of Comets in the Space Age*, ed. W. F. Huebner (Heidelberg: Springer), pp. 113–176.

Grün, E., Peschke, S. B., Boehnhardt, H., Campins, H., Osip, D. J., Hanner, M. S., Heinrichsen, I., Knacke, R., Leinert, Ch., Lemke, D., Lisse, C. M., Stickel, M., Sykes, M., Vanýsek, V., and Zarnecki, J. 1998, in preparation.

Gustafson, B. Å. S. 1989. Comet ejection and dynamics of nonspherical dust particles and meteoroids. *Astrophys. J.* 337:945–949.

Hahn, J. M., Rettig, T. W., and Mumma, M. J. 1996. Comet Shoemaker-Levy 9 dust. *Icarus* 121:291–304.

Hammel, H. B., Telesco, C. M., Campins, H., Decher, R., Storrs, A. D., and Cruikshank, D. P. 1987. Albedo maps of comets P/Halley and P/Giacobini-Zinner. *Astron. Astrophys.* 187:665–668.

Hanner, M. S. 1981. On the detectability of icy grains in the comae of comets. *Icarus* 47:342–350.

Hanner, M. S. 1983. The nature of cometary dust from remote sensing. In *Cometary Exploration*, ed. T. I. Gombosi (Budapest: Hungarian Academy of Sciences), Vol. 2, pp. 1–22.

Hanner, M. S. 1983. Comet Cernis: Icy grains at last? *Astrophys. J.*

277:L75–L78.

Hanner, M. S., and Campins, H. 1986. Thermal emission from the dust coma of comet Bowell and a model for the grains. *Icarus* 67:51–62.

Hanner, M. S., Gehrz, R. D., Harker, D. E., Hayward, T. L., Lynch, D. K., Mason, C. C., Russell, R. W., Williams, D. M., Wooden, D. H., and Woodward, C. E. 1998. Thermal emission from the dust coma of comet Hale-Bopp and the composition of the silicate grains. *Earth Moon Plan.*, submitted.

Hanner, M. S., Giese, R. H., Weiss, K., and Zerull, R. 1981. On the definition of albedo and application to irregular particles. *Astron. Astrophys.* 104:42–46.

Hanner, M. S., Hackwell, J. A., Russell, R. W., and Lynch, D. K. 1994b. Silicate emission feature in the spectrum of comet Mueller 1993a. *Icarus* 112:490–495.

Hanner, M. S., Lynch, D. K., and Russell, R. W. 1994a. The 8–13 micron spectra of comets and the composition of the silicate grains. *Astrophys. J.* 425:274-285.

Hanner, M. S., Lynch, D. K., Russell, R. W., Hackwell, J. A., and Kellogg, R. 1996. Mid-infrared spectra of comets P/Borrelly, P/Faye, and P/Schaumasse. *Icarus* 124:344–351.

Hanner, M. S., and Newburn, R. L. 1989. Infrared photometry of comet Wilson (1986 l) at two epochs. *Astron. J.* 97:254–261.

Hanner, M. S., Newburn, R. L., Gehrz, R. D., Harrison, T., Ney, E. P., and Hayward, T. L. 1990. The infrared spectrum of comet Bradfield (1987s) and the silicate emission feature. *Astrophys. J.* 348:312–321.

Hanner, M. S., Tedesco, E., Tokunaga, A. T., Veeder, G. J., Lester, D. F., Witteborn, F. C., Bregman, J. D., Gradie, J., and Lebofsky, L. 1985. The dust coma of periodic comet Churyumov-Gerasimenko (1982 VIII). *Icarus* 64:11–19.

Hanner, M. S., Tokunaga, A. T. Golisch, W. F., Griep, D. M., and Kaminski, C. D. 1987. Infrared emission from P/Halley's dust coma during March 1986. *Astron. Astrophys.* 187:653–660.

Harding, C. L. 1824. Astronomische Nachrichten, Beobachtungen des diesjährigen Kometen, etc. *Berlin. Astron. Jahrbuch für 1827*, pp. 131–135.

Harmon, J. K., Campbell, D. B., Hine, A. A., Shapiro, I. I., and Marsden, B. G. 1989. Radar observations of comet IRAS-Araki-Alcock 1983d. *Astrophys. J.* 338:1071–1093.

Harmon, J. K., Ostro, S. J., Benner, L. A. M., Rosema, K. D., Jurgens, R. F., Winkler, R., Yeomans, D. K., Choate, D., Cormier, R., Giorgini, J. D., Mitchell, D. L., Chodas, P. W., Rose, R., Kelley, D., Slade, M. A., and Thomas, M. L. 1997. Comet Hyakutake (C/1996 B2): Radar detection of nucleus and coma. *Science* 278:1921–1924.

Hartmann, W. K., and Cruikshank, D. P. 1984. Comet color changes

with solar distance. *Icarus* 57:55–62.

Hartmann, W. K., Cruikshank, D. P., and Degewij, J. 1982. Remote comets and related bodies: VJHK colorimetry and surface materials. *Icarus* 52:377–408.

Hellmich, R. 1981. The influence of the radiation transfer in cometary dust halos on the production rates of gas and dust. *Astron. Astrophys.* 93:341–346.

Hellmich, R., and Keller, H. U. 1981. On the visibility of nuclei of dusty comets. *Icarus* 47:325–332.

Herter, T., Campins, H., and Gull, G. E. 1987. Airborne spectrophotometry of P/Halley from 16 to 30 microns. *Astron. Astrophys.* 187:629–631.

Hevelius, J. 1682. Excerpta ex epistola. II. De cometa anno 1682 mense Augusto & Septimbri viso. *Acta Erudit.*, Dec. 1682, pp. 389–391.

Hewins, R. H. 1988. Experimental studies of chondrules. In *Meteorites and the Early Solar System* , eds. J. F. Kerridge and M. S. Matthews (Tucson: University of Arizona), pp. 660–679.

Horányi, M., and Mendis, D. A. 1986. The effects of electrostatic charging on the dust distribution at Halley's comet. *Astrophys. J.* 307:800–807.

Hornung, K., and Kissel, J. 1994. On shock wave impact ionization of dust particles. *Astron. Astrophys.* 291:324–336.

Hughes, D. W. 1988. Origin of the Solar System. In *Origins*, ed. A. C. Fabian (Cambridge: Cambridge University), pp. 26–68.

Hughes, D. W. 1991. Possible mechanisms for cometary outbursts. In *Comets in the Post-Halley Era*, eds. R. L. Newburn, Jr., M. Neugebauer, and J. Rahe (Dordrecht: Kluwer), pp. 825–851.

Inogamov, N. A. 1987. Electrostatic screening by self-consistent space charge and the ion dynamics in a time-of-flight mass spectrometer. *J. Eng. Phys.* 52:396–403.

Irvine, W. M., and Knacke, R. F. 1989. The chemistry of interstellar gas and grains. In *Origin and Evolution of Planetary and Satellite Atmospheres*, ed. S. K. Atreya et al. (Tucson: University of Arizona), pp. 3–34.

Jaegermann, R. 1903. *Prof. Dr. Th. Bredichin's Mechanische Untersuchungen über Cometenformen.* (St. Petersburg: Voss.)

Jambor, B. J. 1973. The split tail of comet Seki-Lines. *Astrophys. J.* 185:727–734.

Jessberger, E. K. 1993. Über die Zusammensetzung des kometären Staubes. *Mitt. Österreich. Mineralog. Ges.* 138:19–32.

Jessberger, E. K., Christoforidis, A., and Kissel, J. 1988. Aspects of the major element composition of Halley's dust. *Nature* 332:691-695.

Jessberger, E. K., and Kissel, J. 1991. Chemical properties of cometary dust and a note on carbon isotopes. In *Comets in the post-Halley Era*, eds. R. L. Newburn, Jr., M. Neugebauer, and J. Rahe (Dor-

drecht: Kluwer), pp. 1075–1092.

Jessberger, E. K., Kissel, J., Fechtig, H., and Krueger, F. R. 1986. On the average chemical composition of cometary dust. In *Comet Nucleus Sample Return*, ESA SP-249, ed. O. Melita (Noordwijk: ESTEC), pp. 27–30.

Jessberger, E. K., Kissel, J., and Rahe, J. 1989. The composition of comets. In *Origin and Evolution of Planetary and Satellite Atmospheres*, eds. S. K. Atreya, J. B. Pollack, and M. S. Matthews (Tucson: University of Arizona), pp. 167–191.

Jewitt, D. 1990. The persistent coma of comet P/Schwassmann-Wachmann 1. *Astrophys. J.* 351:277–286.

Jewitt, D., and Luu, J. 1990. The submillimeter radio continuum of comet P/Brorsen-Metcalf. *Astrophys. J.* 365:738–747.

Jewitt, D., and Luu, J. 1992. Submillimeter continuum emission from comets. *Icarus* 100:187–196.

Jewitt, D. C., and Matthews, H. E. 1997. Submillimeter continuum observations of comet Hyakutake (1996 B2). *Astron. J.* 113:1145-1151.

Jewitt, D., and Meech, K. J. 1986. Cometary grain scattering versus wavelength, or, "what color is cometary dust?". *Astrophys. J.* 310:937–952.

Jewitt, D., Senay, M., and Matthews, H. 1996. Observations of carbon monoxide in comet Hale-Bopp. *Science* 271:1110–1113.

Jorda, L., Lecacheus, J, and Colas, F. 1997. Comet C/1995 O1 (Hale-Bopp). *IAU Circ.* No. 6583.

Keller, H. U., Delamere, W. A., Huebner, W. F., Reitsema, H. J., Schmidt, H. U., Whipple, F. L., Wilhelm, K., Curdt, W., Kramm, R., Thomas, N., Arpigny, C., Barbieri, C., Bonnet, R. M., Cazes, S., Coradini, M., Cosmovici, C. B., Hughes, D. W., Jamar, C., Malaise, D., Schmidt, K., Schmidt, W. K. H., and Siege, P. 1987. Comet P/Halley's nucleus and its activity. *Astron. Astrophys.* 187:807–823.

Keller, H. U., Marconi, M. L., and Thomas, N. 1990. Hydrodynamic implications of particle fragmentation near cometary nuclei. *Astron. Astrophys.* 227:L1–L4.

Keller, H. U., and Thomas, N. 1989. Evidence for near-surface breezes on comet P/Halley. *Astron. Astrophys.* 226:L9–L12.

Khare, B. N., Arakawa, E. T., Meisse, C., Thompson, W. R., Sagan, C., Gilmour, I., and Anders, E. 1990. Optical constants of kerogen from 0.15 to 40 $\mu$m. In *First International Conference on Laboratory Research for Planetary Atmospheres*, NASA CP–3077 (Washington D.C.: National Aeronautics and Space Administration), pp. 340–356.

Kikuchi, S., Mikami, Y., Mukai, T., Mukai, S., and Hough, J. H. 1987. Polarimetry of comet P/Halley. *Astron. Astrophys.* 187:689–692.

Kimura, H., and Liu, C.-p. 1977. On the structure of cometary dust tails. *Chinese Astron.* 1:235–264.

Kirch, G. 1681. *Neuen Himmelszeitung, darinn sonderlich und ausführlich von den zwey neuen grossen im Jahr 1680 erschienenen Cometen, etc.* (Nürnberg), p. 62.

Kissel, J. 1986a. The Giotto particulate impact analyser. In *The Giotto Mission — Its Scientific Investigations*, ESA SP-1077, eds. R. Reinhard and B. Battrick (Noordwijk: ESTEC), pp. 67–83.

Kissel, J. 1986b. Mass spectrometric studies of Halley comet. *Adv. Mass Spectr. 1985*, pp. 175–184.

Kissel, J., Brownlee, D. E., Büchler, K., Clark, B. C., Fechtig, H., Grün, E., Hornung, K., Igenbergs, E. B., Jessberger, E. K., Krueger, F. R., Kuczera, H., McDonnell, J. A. M., Morfill, G. M., Rahe, J., Schwehm, G. H., Sekanina, Z., Utterback, N. G., Völk, H. J., and Zook, H. A. 1986a. Composition of comet Halley dust particles from Giotto observations. *Nature* 321:336–338.

Kissel, J., and Krueger, F. R. 1987a. The organic component in dust from comet Halley as measured by the PUMA mass spectrometer on board Vega 1. *Nature* 326:755–760.

Kissel, J., and Krueger, F. R. 1987b. Ion formation by impact of fast dust particles and comparison with related techniques. *Appl. Phys. A* 42:69–85.

Kissel, J., Sagdeev, R. Z., Bertaux, J. L., Angarov, V. N., Audouze, J., Blamont, J. E., Büchler, K., Evlanov, E. N., Fechtig, H., Fomenkova, M. N., von Hoerner, H., Inogamov, N. A., Khromov, V. N., Knabe, W., Krueger, F. R., Langevin, Y., Leonas, V. B., Levasseur-Regourd, A. C., Managadze, G. G., Podkolzin, S. N., Shapiro, V. D., Tabaldyev, S. R., and Zubkov, B. V. 1986b. Composition of comet Halley dust particles from Vega observations. *Nature* 321:280–282.

Kitamura, Y. 1986. Axisymmetric dusty gas jet in the inner coma of a comet. *Icarus* 66:241–257.

Kitamura, Y. 1987. Axisymmetric dusty gas jet in the inner coma of a comet. II. The case of isolated jets. *Icarus* 72:555–567.

Koike, C., Shibai, H., and Tuchiyama, A. 1993. Extinction of olivine and pyroxene in mid- and far-infrared regions. *Mon. Not. R. Astron. Soc.* 264:654–658.

Kömle, N. I. 1990. Jet and shell structures in the cometary coma: modelling and observations. In *Comet Halley: Investigations, Results, Interpretations*, ed. J. W. Mason (Chichester: Ellis Horwood), Vol. 1, pp. 231–243.

Kömle, N. I., and Ip, W.-H. 1987a. Anisotropic non-stationary gas flow dynamics in the coma of comet P/Halley. *Astron. Astrophys.* 187:405–410.

Kömle, N. I., and Ip, W.-H. 1987b. A model for the anisotropic struc-

ture of the neutral gas coma of a comet. In *Diversity and Similarity of Comets*, ESA SP-278, eds. E. J. Rolfe and B. Battrick (Noordwijk: ESTEC), pp. 247–254.

Körösmezey, A., and Gombosi, T. I. 1990. A time-dependent dusty gas dynamic model of axisymmetric cometary jets. *Icarus* 84:118–153.

Krankowsky, D., and Eberhardt, P. 1990. Evidence for the composition of ices in the nucleus of comet Halley. In *Comet Halley: Worldwide Investigations, Results, Interpretations*, ed. J. Mason (Chichester: Ellis Horwood), pp. 273–289.

Lamy, P. 1986a. Ground-based observations of the dust emission from comet Halley. *Adv. Space Res.* 5:(12)317–(12)323.

Lamy, P. L. 1986b. Cometary dust: Observational evidences and properties. In *Asteroids, Comets, Meteors II*, eds. C.-I. Lagerkvist, B. A. Lindblad, H. Lundstedt, and H. Rickman (Uppsala: University of Uppsala), pp. 373–388.

Lamy, P. L., and Perrin, J.-M. 1986. Volume scattering function and space distribution of the interplanetary dust cloud. *Astron. Astrophys.* 163:269–286.

Langevin, Y., Kissel, J., Bertaux, J.-L., and Chassefière, E. 1987. First statistical analysis of 5000 mass spectra of cometary grains obtained by PUMA 1 (Vega 1) and PIA (Giotto) impact ionization mass spectrometers in the compressed modes. *Astron. Astrophys.* 187:779–784.

Larson, S. M. 1978. A rotation model for the spiral structure in the coma of comet Bennett (1970 II). *Bull. Am. Astron. Soc.* 10:589. (Abstract.)

Larson, S. M., and Minton, R. B. 1972. Photographic observations of comet Bennett, 1970 II. In *Comets: Scientific Data and Missions*, eds. G. P. Kuiper and E. Roemer (Tucson: University of Arizona), pp. 183–208.

Lawler, M., and Brownlee, D. 1992. CHON as a component of dust from comet Halley. *Nature* 359:810–812.

Lawler, M. E., Brownlee, D. E., Temple, S., and Wheelock, M. M. 1989. Iron, magnesium, and silicon in dust from Comet Halley. *Icarus* 80:225–242.

Levasseur-Regourd, A.-Ch., Hadamcik, E., and Renard, J. B. 1996. Evidence for two classes of comets from their polarimetric properties at large phase angles. *Astron. Astrophys.* 313:327–333.

Lien, D. J. 1991. Optical properties of cometary dust. In *Comets in the Post-Halley Era*, eds. R. L. Newburn, Jr., M. Neugebauer, and J. Rahe (Dordrecht: Kluwer), pp. 1005–1041.

Lisse, C. M., A'Hearn, M. F., Hauser, M. G., Kelsall, T., Lien, D. J., Moseley, S. H., Reach, W. T., and Silverberg, R. F. 1998. Infrared observations of comets by COBE. *Astrophys. J.*, in press.

Lisse, C. M., Freudenreich, H. T., Hauser, M. G., Kelsall, T., Moseley,

S. H., Reach, W. T., and Silverberg, R. F. 1994. Infrared observations of comet Austin (1990 V) by the COBE: Diffuse Infrared Background Experiment. *Astrophys. J.* 432:L71–L74.

Lynch, D. K., Hanner, M. S., and Russell, R. W. 1992a. 8–13 $\mu$m spectroscopy and IR photometry of comet P/Brorsen-Metcalf (1989o) near perihelion. *Icarus* 97:269-275.

Lynch, D. K., Russell, R. W., Campins, H., Witteborn, F. C., Bregman, J. D., Rank, D. W., and Cohen, M. C. 1989. 5–13 $\mu$m airborne observations of comet Wilson 1986l. *Icarus* 82:379–388.

Lynch, D. K., Russell, R. W., Hackwell, J. A., Hanner, M. S., and Hammel, H. B. 1992b. 8- to 13-$\mu$m spectroscopy of comet Levy 1990 XX. *Icarus* 100:197–202.

Maas, D., Krueger, F. R., and Kissel, J. 1989. Mass and density of silicate- and CHON-type dust particles released by comet P/Halley. In *Asteroids, Comets, Meteors III*, eds. C.-I. Lagerkvist, H. Rickman, B. A. Lindblad, and M. Lindgren (Uppsala: Uppsala Universitet), pp. 389–392.

Marconi, M. L., and Mendis, D. A. 1983. The atmosphere of a dirty-clathrate cometary nucleus: a two-phase, multifluid model. *Astrophys. J.* 273:381–396.

Marconi, M. L., and Mendis, D. A. 1984. The effects of the diffuse radiation fields due to multiple scattering and thermal reradiation by dust on the dynamics and thermodynamics of a dusty cometary atmosphere. *Astrophys. J.* 287:445–454.

Marsden, B. G. 1989. The sungrazing comet group. II. *Astron. J.* 98:2306–2321.

McDonald, G. D., Whited, L. J., DeRuiter, C., Khare, B. N., Patnaik, A., and Sagan, C. 1996. Production and chemical analysis of cometary ice tholins. *Icarus* 122:107–117.

McDonnell, J. A. M., ed. 1978. *Cosmic Dust.* (New York: Wiley.)

McDonnell, J. A. M., Lamy, P. L., and Pankiewicz, G. S. 1991. Physical properties of cometary dust. In *Comets in the Post-Halley Era*, eds. R. L. Newburn, Jr., M. Neugebauer, and J. Rahe (Dordrecht: Kluwer), pp. 1043–1073.

Meech, K. J., and Jewitt, D. C. 1987. Observations of comet P/Halley at minimum phase angle. *Astron. Astrophys.* 187:585–593.

Merrill, K. M. 1974. 8-13 $\mu$m spectrophotometry of comet Kohoutek. *Icarus* 23:566–567.

Millis, R. L., A'Hearn, M. F., and Thompson, D. T. 1982. Narrowband photometry of comet P/Stephan-Oterma and the backscattering properties of cometary grains. *Astron. J.* 87:1310–1317.

Moiseyev, N. D. 1925. Über den Schweif des Kometen 1901 I. *Russ. Astron. J.* 2:73–84.

Mukhin, L. M., Dolnikov, G. A., Evlanov, E. N., Fomenkova, M. N., Prilutskii, O. F., and Sagdeev, R. Z. 1991. Re-evaluation of the

chemistry of dust grains in the coma of comet Halley. *Nature* 350:480–481.

Needham, J., Beer, A., and Ho, P.-Y. 1957. "Spiked" comets in ancient China. *Observatory* 77:137–138.

Ney, E. P. 1974. Multiband photometry of comets Kohoutek, Bennett, Bradfield, and Encke. *Icarus* 23:551–560.

Ney, E. P. 1982. Optical and infrared observations of bright comets in the range 0.5 $\mu$m to 20 $\mu$m. In *Comets*, ed. L. L. Wilkening (Tucson: University of Arizona), pp. 323–340.

Ney, E. P., and Merrill, K. M. 1976. Comet West and the scattering function of cometary dust. *Science* 194:1051–1053.

Nishioka, K., Saito, K., Watanabe, J.-i., and Ozeki, T. 1992. Photographic observations of the synvhronic band in the tail of comet West 1976 VI. *Publ. Nat. Astron. Obs. Japan* 2:601–621.

Nishioka, K., and Watanabe, J.-i. 1990. Finite lifetime fragment model for synchronic band formation in dust tails of comets. *Icarus* 87:403–411.

Norton, W. A. 1844. On the mode of formation of the tails of comets. *Am. J. Sci. Arts* 46:104–129.

Norton, W. A. 1861. Theoretical determination of the dimensions of Donati's comet. *Am. J. Sci. Arts* (Ser. 2) 32:54–71.

Notni, P. 1964. Eigenschaften und Bewegung der Staubteilchen in Koma und Schweif von Kometen. *Veröff. Sternw. Babelsberg* 15, No. 1, pp. 1–51.

Notni, P. 1966. On the forces acting on charged dust particles in cometary atmospheres. *Mém. Soc. R. Sci. Liège* (Ser. 5), 12:379–383.

Notni, P., and Thänert, W. 1988. The striae in the dust tails of great comets — a comparison to various theories. *Astron. Nachr.* 309:133–146.

Notni, P., and Tiersch, H. 1987. Charging of dust particles in comets and in interplanetary space. *Astron. Astrophys.* 187:796–800.

Olbers, H. W. M. 1825. (Extract from a letter.) *Astron. Nachr.* 3:5–10.

Olbers, H. W. M. 1831. Ueber anomale Cometenschweife. *Astron. Nachr.* 8:469–472.

Orlov, S. V. 1928. The mechanical theory of cometary forms. *Publ. Inst. Astrophys. Russ.* 3, No. 4, pp. 1–77. (In Russian.)

Orlov, S. V. 1929. The mechanical theory of cometary forms. *Russ. Astron. J.* 6:180–186.

Orlov, S. V. 1960. *On the Nature of Comets.* (Moscow: Akad. Nauk.)

Pansecchi, L., and Fulle, M. 1990. A neck-line structure in the dust tail of the Great January Comet 1910 I. *Astron. Astrophys.* 239:369–374.

Pansecchi, L., Fulle, M., and Sedmak, G. 1987. The nature of two anomalous structures observed in the dust tail of comet Bennett

1970 II: a possible neck-line structure. *Astron. Astrophys.* 176:358–366. [Erratum: 1988, *Astron. Astrophys.* 205:367.]

Parker, E. N. 1958. Dynamics of the interplanetary gas and magnetic fields. *Astrophys. J.* 128:664–676.

Parker, E. N. 1963. *Interplanetary Dynamical Processes.* (New York: Interscience.) 272 pp.

Peschke, S. B., Grün, E., Boehnhardt, H., Campins, H., Osip, D. J., Hanner, M. S., Heinrichsen, I., Knacke, R., Leinert, Ch., Lemke, D., Lisse, C. M., Stickel, M., Sykes, M., Vanýsek, V., and Zarnecki, J. 1998. ISOPHOT observations of comet Hale-Bopp: first results. *Earth Moon Plan.*, submitted.

Pittichová, J., Sekanina, Z., Birkle, K., Boehnhardt, H., Engels, D., and Keller, P. 1998. An early investigation of the striated tail of comet Hale-Bopp (C/1995 O1). *Earth Moon Plan.*, submitted; JPL Cometary Science Team Preprint Series No. 174.

Prinn, R., and Fegley, B. 1989. Solar nebula chemistry: origin of planetary satellite, and cometary volatiles. In *Origin and Evolution of Planetary and Satellite Atmospheres*, eds. S. K. Atreya, J. B. Pollack, and M. S. Matthews (Tucson: University of Arizona), pp. 78–136.

Probstein, R. F. 1969. The dusty gasdynamics of comet heads. In *Problems of Hydrodynamics and Continuum Mechanics*, eds. F. Bisshopp et al. (Philadelphia: Soc. Ind. Appl. Math.), pp. 568–583.

Rahe, J., Donn, B., and Wurm, K. 1969. *Atlas of Cometary Forms.* NASA SP-198. (Washington, D.C.: National Aeronautics and Space Administration.)

Rettig, T. W., and Hahn, J. M. 1997. Comet Shoemaker-Levy 9: an active comet. *Planet. Space Sci.* 45:1271–1277.

Rettig, T. W., Tegler, S. C., Pasto, D. J., and Mumma, M. J. 1992. Comet outbursts and polymers of HCN. *Astrophys. J.* 398:293–298.

Reuter, D. C. 1992. The contribution of methanol to the 3.4 $\mu$m emission feature in comets. *Astrophys. J.* 386:330–335.

Richter, K., and Keller, H. U. 1987. Density and brightness distribution of cometary dust tails. *Astron. Astrophys.* 171:317–326.

Richter, K., and Keller, H. U. 1988. The anomalous dust tail of comet Kohoutek (1973 XII) near perihelion. *Astron. Astrophys.* 206:136–142.

Rieke, G. H., and Lee, T. A. 1974. Photometry of comet Kohoutek (1973f). *Nature* 248:737–740.

Rietmeijer, F., Mukhin, L. M., Fomenkova, M. N., and Evlanov, E. N. 1989. Layer silicate chemistry in P/comet Halley from PUMA-2 data. *Lunar Planet. Sci. Conf.* 20:904–905.

Rose, L. A. 1979. Laboratory simulation of infrared astrophysical features. *Astrophys. Space Sci.* 65:47–67.

Ryan, E. V., and Campins, H. 1991. Comet Halley spatial and temporal variability of the silicate emission feature. *Astron. J.* 101:695–705.

Sagdeev, R. Z., Evlanov, E. N., Fomenkova, M. N., Mukhin, L. M., Prilutskii, O. F., and Zubkov, B. V. 1987. Composition of comet Halley dust particles based on PUMA instruments measurements in zero mode. *Space Res.* 25:849–855.

Sagdeev, R. Z., Evlanov, E. N., Fomenkova, M. N., Prilutskii, O. F., and Zubkov, B. V. 1989. Small-size dust particles near Halley's comet. *Adv. Space Res.* 9:(3)263-(3)267.

Sandford, S. A., and Walker, R. M. 1985. Laboratory infrared transmission spectra of individual interplanetary dust particles from 2.5 to 25 microns. *Astrophys. J.* 291:838–851.

Schulze, H., Kissel, J., and Jessberger, E. 1996. Chemistry and mineralogy of comet Halley's dust. In *From Stardust to Planetesimals*, Conf. Series Vol. 122, eds. Y. Pendleton and A. Tielens (San Francisco: Astronomical Society of the Pacific), pp. 397–414.

Schwarzschild, K. 1901. Der Druck des Lichtes auf kleine Kugeln und die Arrhenius'sche Theorie des Cometenschweife. *Sitz. Bayer. Akad. Wiss. München 1901*, pp. 293–327.

Schwehm, G. 1976. Radiation pressure on interplanetary dust particles. In *Interplanetary Dust and Zodiacal Light*, eds. H. Elsässer and H. Fechtig (Berlin: Springer), pp. 459–463.

Schwehm, G., and Rohde, M. 1977. Dynamical effects on circumsolar dust grains. *J. Geophys.* 42:727–735.

Sekanina, Z. 1973. Comet Kohoutek (1973f). *IAU Circ.* No. 2580.

Sekanina, Z. 1976. Progress in our understanding of cometary dust tails. In *The Study of Comets*, NASA SP-393, eds. B. Donn, M. Mumma, W. Jackson, M. A'Hearn, and R. Harrington (Washington, D.C.: National Aeronautics and Space Adnministration), pp. 893–939.

Sekanina, Z. 1979. Fan-shaped coma, orientation of rotation axis, and surface structure of a cometary nucleus. *Icarus* 37:420–442.

Sekanina, Z. 1980. Physical characteristics of cometary dust from dynamical studies: a review. In *Solid Particles in the Solar System*, eds. I. Halliday and B. A. McIntosh (Dordrecht: Reidel), pp. 237–250.

Sekanina, Z. 1981a. Distribution and activity of discrete emission areas on the nucleus of periodic comet Swift-Tuttle. *Astron. J.* 86:1741–1773.

Sekanina, Z. 1981b. Properties of dust particles in comet Halley from observations made in 1910 during its encounter with the Earth. In *The Comet Halley Dust & Gas Environment*, ESA SP-174, eds. B. Battrick and E. Swallow (Noordwijk: ESTEC), pp. 55–65.

Sekanina, Z. 1981c. Rotation and precession of cometary nuclei. *Ann. Rev. Earth Planet Sci.* 9:113–145.

Sekanina, Z. 1982a. The problem of split comets in review. In *Comets*, ed. L. L. Wilkening (Tucson: University of Arizona), pp. 251–287.

Sekanina, Z. 1982b. The path and surviving tail of a comet that fell into the Sun. *Astron. J.* 87:1059–1072.

Sekanina, Z. 1986. Periodic comet Halley (1982i). *IAU Circ.* No. 4187.

Sekanina, Z. 1987a. Anisotropic emission from comets: Fans versus jets. I. Concept and modeling. In *Diversity and Similarity of Comets*, ESA SP-278, eds. E. J. Rolfe and B. Battrick (Noordwijk: ESTEC), pp. 315–322.

Sekanina, Z. 1987b. Anisotropic emission from comets: Fans versus jets. II. Periodic comet Tempel 2. In *Diversity and Similarity of Comets*, ESA SP-278, eds. E. J. Rolfe and B. Battrick (Noordwijk: ESTEC), pp. 323–336.

Sekanina, Z. 1991a. Cometary activity, discrete outgassing areas, and dust-jet formation. In *Comets in the Post-Halley Era*, eds. R. L. Newburn, Jr., M. Neugebauer, and J. Rahe (Dordrecht: Kluwer), pp. 769–823.

Sekanina, Z. 1991b. Randomization of dust-ejecta motions and the observed morphology of cometary heads. *Astron. J.* 102:1870–1878.

Sekanina, Z. 1993. Computer simulation of the evolution of dust coma morphology in an outburst: P/Schwassmann-Wachmann 1. In *On the Activity of Distant Comets*, eds. W. F. Huebner, H. U. Keller, D. Jewitt, J. Klinger, and R. M. West (San Antonio: Southwest Research Institute), pp. 166–181.

Sekanina, Z. 1995. Evidence on sizes and fragmentation of the nuclei of comet Shoemaker-Levy 9 from Hubble Space Telescope images. *Astron. Astrophys.* 304:296–316.

Sekanina, Z. 1996a. Tidal breakup of the nucleus of comet Shoemaker-Levy 9. In *The Collision of Comet P/Shoemaker-Levy 9 and Jupiter*, eds. K. S. Noll, H. A. Weaver, and P. D. Feldman (Cambridge: Cambridge University), pp. 55–80.

Sekanina, Z. 1996b. Morphology of cometary dust coma and tail. In *Physics, Chemistry, and Dynamics of Interplanetary Dust*, Conf. Series Vol. 104, eds. B. Å. S. Gustafson and M. S. Hanner (San Francisco: Astronomical Society of the Pacific), pp. 377–382.

Sekanina, Z. 1996c. Activity of comet Hale-Bopp (1995 O1) beyond 6 AU from the Sun. *Astron. Astrophys.* 314:957–965.

Sekanina, Z. 1998. Modeling the diurnal evolution of a dust feature in comet Hale-Bopp (1995 O1). *Astrophys. J.* 494:L121–L124.

Sekanina, Z., and Boehnhardt, H. 1998. Dust morphology of comet Hale-Bopp (C/1995 O1). II. Introduction of a working model. *Earth Moon Plan.*, submitted; JPL Cometary Science Team Preprint Series No. 176.

Sekanina, Z., Chodas, P. W., and Yeomans, D. K. 1994. Tidal disruption and the appearance of periodic comet Shoemaker-Levy 9.

*Astron. Astrophys.* 289:607–636.

Sekanina, Z., Chodas, P. W., and Yeomans, D. K. 1998. Secondary fragmentation of comet Shoemaker-Levy 9 and the ramifications for the progenitor's breakup in July 1992. *Planet. Space Sci.*, in press.

Sekanina, Z., and Farrell, J. A. 1978. Comet West 1976 VI: discrete bursts of dust, split nucleus, flare-ups, and particle evaporation. *Astron. J.* 83:1675–1680.

Sekanina, Z., and Farrell, J. A. 1980. The striated dust tail of comet West 1976 VI as a particle fragmentation phenomenon. *Astron. J.* 85:1538–1554.

Sekanina, Z., and Farrell, J. A. 1982. Two dust populations of particle fragments in the striated tail of comet Mrkos 1957 V. *Astron. J.* 87:1836–1853.

Sekanina, Z., and Farrell, J. A. 1986. The striated dust tail of comet 1910 I. *Bull. Am. Astron. Soc.* 18:818. (Abstract.)

Sekanina, Z., and Larson, S. M. 1984. Coma morphology and dust-emission pattern of periodic comet Halley. II. Nucleus spin vector and modeling of major dust features in 1910. *Astron. J.* 89:1408–1425, 1446–1447.

Sekanina, Z., and Larson, S. M. 1986a. Coma morphology and dust-emission pattern of periodic comet Halley. IV. Spin vector refinement and map of discrete dust sources for 1910. *Astron. J.* 92:462–482.

Sekanina, Z., and Larson, S. M. 1986b. Dust jets in comet Halley observed by Giotto and from the ground. *Nature* 321:357–361.

Sekanina, Z., Larson, S. M., Hainaut, O., Smette, A., and West, R. M. 1992. Major outburst of periodic comet Halley at a heliocentric distance of 14 AU. *Astron. Astrophys.* 263:367–386.

Sekanina, Z., and Miller, F. D. 1973. Comet Bennett (1970 II). *Science* 179:565–567.

Sekanina, Z., and Pittichová, J. 1998. Distribution law for particle fragmentation times in a theory for striated tails of dust comets: application to comet Hale-Bopp (C/1995 O1). *Earth Moon Plan.*, submitted; JPL Cometary Science Team Preprint Series No. 175.

Sekanina, Z., and Schuster, H. E. 1978. Meteoroids from periodic comet d'Arrest. *Astron. Astrophys.* 65:29–35.

Simpson, J. A., Rabinowitz, D., Tuzzolino, A. J., Ksanfomality, L. V., and Sagdeev, R. Z. 1986. Halley's comet coma dust particle mass spectra, flux distributions, and jet structures derived from measurements on the Vega-1 and Vega-2 spacecraft. In *Exploration of Halley's Comet*, ESA SP-250, eds. B. Battrick, E. J. Rolfe, and R. Reinhard (Noordwijk: ESTEC), Vol. 2, pp. 11–16.

Simpson, J. A., Rabinowitz, D., Tuzzolino, A. J., Ksanfomality, L. V., and Sagdeev, R. Z. 1987. The dust coma of comet P/Halley: mea-

surements on the Vega-1 and Vega-2 spacecraft. *Astron. Astrophys.* 187:742–752.

Simpson, J. A., Tuzzolino, A. J., Ksanfomality, L. V., Sagdeev, R. Z., and Vaisberg, O. L. 1989. Confirmation of dust clusters in the coma of comet Halley. *Adv. Space Res.* 9:(3)259–(3)262.

Snyder, L. E., Webber, J. C., Cruthcher, R. M., and Swenson, G. W., Jr. 1976. Radio observationss of OH in comet West 1975n. *Astrophys. J.* 209:L49–L52.

Šolc, M., Jessberger, E. K., Hsiung, P., and Kissel, J. 1987. Halley dust composition. *Publ. Astron. Inst. Czech. Acad. Sci.* No. 67, pp. 47–50.

Šolc, M., Vanýsek, V., and Kissel, J. 1986. Carbon stable isotopes in comets after encounters with P/Halley. In Exploration of Halley's Comet, ESA SP-250, eds. B. Battrick, E. J. Rolfe, and R. Reinhard (Noordwijk: ESTEC), Vol. 1, pp. 373–376.

Solem, J. C. 1995. Cometary breakup calculations based on a gravitationally-bound agglomeration model: the density and size of Shoemaker-Levy 9. *Astron. Astrophys.* 302:596–608.

Southworth, R. B. 1963. Dust in comet Arend-Roland. *Astron. J.* 68:293–294.

Southworth, R. B. 1964. The size distribution of the zodiacal particles. *Ann. New York Acad. Sci.* 119:54–67.

Stephens, J. R., and Russell, R. W. 1979. Emission and extinction of ground and vapor-condensed silicates from 4 to 14 microns and the 10 micron silicate feature. *Astrophys. J.* 228:780–786.

Sykes, M. V., Lebofsky, L. A., Hunten, D. M., and Low, F. J. 1986. The discovery of dust trails in the orbits of periodic comets. *Science* 232:1115–1117.

Sykes, M. V., Lien, D. J., and Walker, R. G. 1990. The Tempel 2 dust trail. *Icarus* 86:236–247.

Tanigawa, T., Kawakita, H., and Watanabe, J.-i. 1997. The activity of the fragmented nucleus of comet Shoemaker-Levy 9. *Planet. Space Sci.* 45:1417–1422.

Telesco, C. M., Decher, R., Baugher, C., Campins, H., Mozurkewich, D., Thronson, H. A., Cruikshank, D. P., Hammel, H. B., Larson, S., and Sekanina, Z. 1986. Thermal-infrared and visual imaging of comet Giacobini-Zinner. *Astrophys. J.* 310:L61–L65.

Thomas, N., and Keller, H. U. 1987. Comet P/Halley's near-nucleus jet activity. In *Diversity and Similarity of Comets*, ESA SP-278, eds. E. J. Rolfe and B. Battrick (Noordwijk: ESTEC), pp. 337–342.

Tielens, A. G. G. M., and Allamandola, L. 1987. Composition, structure and chemistry of interstellar dust. In *Interstellar Processes*, eds. D. Hollenbach and H. Thronson (Dordrecht: Reidel), pp. 397–469.

Tiersch, H., and Notni, P. 1989. The electric potential on dust particles

in comets and in interplanetary space. *Astron. Nachr.* 310:67–78.

Tokunaga, A. T., Golisch, W. F., Griep, D. M., Kaminski, C. D., and Hanner, M. S. 1986. The NASA Infrared Telescope Facility comet Halley monitoring program I. Preperihelion results. *Astron. J.* 92:1183–1190.

Tokunaga, A. T., Golisch, W. F., Griep, D. M., Kaminski, C. D., and Hanner, M. S. 1988. The NASA Infrared Telescope Facility comet Halley monitoring program II. Postperihelion results. *Astron. J.* 96:1971–1976.

Tokunaga, A. T., Hanner, M. S., Golisch, W. F., Griep, D. M., Kaminski, C. D., and Chen, H. 1992. Infrared monitoring of comet P/Tempel 2. *Astron. J.* 104:1611–1617.

Utterback, N. G., and Kissel, J. 1990. Attogram dust cloud a million kilometers from comet Halley. *Astron. J.* 100:1315-1322.

Walker, R. G., and Aumann, H. H. 1984. IRAS observations of cometary dust. *Adv. Space Res.* 4:(9)197–(9)201.

Watanabe, J.-i., and Nishioka, K. 1991. Synchronic band and its implication in the cometary dust. In *Origin and Evolution of Interplanetary Dust*, eds. A. C. Levasseur-Regourd and H. Hasegawa (Dordrecht: Kluwer), pp. 253–256.

Weaver, H. A., A'Hearn, M. F., Arpigny, C., Boice, D. C., Feldman, P. D., Larson, S. M., Lamy, P., Levy, D. H., Marsden, B. G., Meech, K. J., Noll, K. S., Scotti, J. V., Sekanina, Z., Shoemaker, E. M., Shoemaker, E. M., Smith, T. E., Stern, S. A., Storrs, A. D., Trauger, J. T., Yeomans, D. K., and Zellner, B. 1995. The Hubble Space Telescope (HST) observing campaign on comet Shoemaker-Levy 9. *Science* 267:1282–1288.

Weaver, H. A., Feldman, P. D., A'Hearn, M. F., Arpigny, C., Brandt, J. C., Festou, M. C., Haken, M., McPhate, J. B., Stern, S. A., and Tozzi, G. P. 1997. The activity and size of the nucleus of comet Hale-Bopp (C/1995 O1). *Science* 275:1900–1904.

Whipple, F. L. 1950. A comet model. I. The acceleration of comet Encke. *Astrophys. J.* 111:375–394.

Whipple, F. L. 1951. A comet model. II. Physical relations for comets and meteors. *Astrophys. J.* 113:464–474.

Whipple, F. L. 1978. Rotation period of comet Donati. *Nature* 273: 134–135.

Whipple, F. L., and Sekanina, Z. 1979. Comet Encke: Precession of the spin axis, nongravitational motion, and sublimation. *Astron. J.* 84:1894–1909.

Williams, D. M., Mason, C. G., Gehrz, R. D., Jones, T. J., Woodward, C. E., Harker, D. E., Hanner, M. S., Wooden, D. H., Witteborn, F. C., and Butner, H. M. 1997. Measurement of submicron grains in the coma of comet Hale-Bopp C/1995 O1 during 1997 February 15–20 UT. *Astrophys. J.* 489:L91–L94.

Wooden, D. H., Harker, D. E., Woodward, C. E., Koike, C., and Butner, H. M. 1998. Discovery of Mg-rich pyroxenes in comet C/1995 O1 (Hale-Bopp): pristine grains revealed at perihelion. *Earth Moon Plan.*, submitted.

Xing, Z., and Hanner, M. S. 1997. Light scattering by aggregate particles. *Astron. Astrophys.* 324:805–820.

Yanamandra-Fisher, P., and Hanner, M. S. 1998. Optical properties of non-spherical particles of size comparable to the wavelength of light: application to comet dust. *Icarus*, submitted.

Yavnel, A. A. 1977. Chemical composition of meteors and meteoritic matter. In *Comets, Asteroids, Meteorites*, ed. A. H. Delsemme (Toledo: University of Toledo), pp. 133–135.

Zinner, E., Wopenka, B., Amari, S., and Anders, E. 1990. Interstellar graphite and other carbonaceous grains from the Murchison meteorite: structure, composition and isotopes of C, N, and Ne. *Lunar Planet. Sci. Conf.* 21:1379–1380.

## FIGURE CAPTIONS

Figure 1. Effects of the spin rate on the evolution of dust ejecta from a point-like source on the equator of a rotating nucleus. The spin axis is normal to the comet's orbit plane (the plane of the figure). The source is active from sunrise ($\Theta_b = -90°$) to sunset ($\Theta_e = +90°$) and all particles are ejected with the same velocity of 500 m/s and subjected to the same solar radiation-pressure acceleration of 0.25 cm/s$^2$. The circles show the position of the nucleus and the curves describe the loci of particles ejected at various times after the onset of emission, $t - t_b$. The sense of rotation and the direction to the Sun are also indicated. The left-hand side of the figure depicts the case of a rapidly rotating nucleus; the right-hand side, of a slowly rotating nucleus. Note the scale differences for the early (top) and late (bottom) phases of evolution. (From Sekanina and Larson 1984.)

Figure 2. Computer generated images of a dust coma consisting of a set of sunward, nearly concentric halos, simulating the appearance of comets such as Donati (C/1858 L1) or Hale-Bopp (C/1995 O1). All the images were generated with identical reference parameters, except for the two randomization constants, $\alpha_1$ and $\alpha_2$. Random noise that is independent of the particle residence length in the coma increases from the left to the right, while the noise that scales with residence length increases from the top to the bottom, $\alpha_2$ characterizing this noise at 1 arcmin from the nucleus. Each frame is about 100 arcsec on a side. The image in the upper left corner ($\alpha_1 = \alpha_2 = 0$), which shows the direction to the Sun, consists of noiseless (deterministic) particle loci. The meaning of the parameters $\alpha_1$ and $\alpha_2$ is explained in the original study. (From Sekanina 1991b.)

Figure 3. Figure 3. Modeling the diurnal evolution of a dust jet in comet Hale-Bopp (C/1995 O1). *Left panel*: selected frames from the jet's animation sequence taken by Jorda et al. (1997) with a 105-cm telescope at Pic du Midi between 3:50 and 15:35 UTC on February 28, 1997. A complete rotation cycle (~11.35 hours) is covered. The image in the upper left corner corresponds to ~12:15 UTC. The temporal separation between neighboring frames, each 32,400 km on a side at the comet, is ~30 minutes. (Original images courtesy of L. Jorda, J. Lecacheux, and F. Colas.) *Right panel*: computer-generated images simulating the observations in the left panel on the assumption that the jet emanated from a discrete source on the nucleus. There is a one-to-one correspondence between the frames in the two panels. The times are reckoned from the source's activation time. The dust ejecta were expanding with velocities of up to 600 m/s. The first frame shows the projected directions of the spin vector ($\omega$) and the Sun (circled dot). (From Sekanina 1998.)

Figure 4. Computer-generated images of comet Hale-Bopp (C/1995 O1), simulating morphology of the dust coma consisting of a radial jet and a spiral arm, for selected times following each of the three emission events that took place between late August and late October 1995. The synthetic image for September 26 can be compared with an image taken then with the Planetary mode Wide Field Planetary Camera-2 of the Hubble Space Telescope (cf. Weaver et al. 1997). Note that the scale for the Event 1 images differs from the scales for the other two events. North is always up and east to the left. (From Sekanina 1996c.)

Figure 5. The photographs of comet Mrkos (C/1957 P1) taken by J. A. Farrell with a 19-cm Schmidt camera near Fort Worth, Texas, on four

consecutive days in August 1957. The original exposures are in the upper row, the digitally processed images in the lower row. The arrow on the first image points to the north. The scale refers to the distances projected onto the plane of the sky at the comet's nucleus. The long narrow tail directed to the upper left is the plasma tail. The striae of the first kind are the long, narrow streaks situated in the left part of the broad, dust tail. The striae of the second kind are the short, stubby bands located further to the right end of the dust tail. (From Sekanina and Farrell 1982.)

Figure 6. A 440 second exposure of comet Shoemaker-Levy 9 (D/1993 F2) taken by J. V. Scotti with the University of Arizona's 91-cm Spacewatch telescope on March 30, 1993. The field is 9 arcmin on a side. North is up and east to rhe left. The nuclear train, the two dust trails, and the wide sector of material with embedded tails are identified. (From Sekanina et al. 1994; original image courtesy of J. V. Scotti, Lunar and Planetary Laboratory.)

Figure 7. Equilibrium temperature versus heliocentric distance for glassy carbon spheres, with radii 0.1–5 $\mu$m. Dash-dot curve is for perfect blackbody.

Figure 8. Equilibrium temperature versus heliocentric distance for glassy silicate spheres, radius 0.5 $\mu$m, with differing absorption. — - — - — $k = 0.001$; — — — $k = 0.01$; - - - - - olivine glass, Mg/Fe = 1 (Dorschner et al. 1995); ——— glassy carbon; — · — · — blackbody.

Figure 9. Silicate emission feature in dusty comets: flux divided by blackbody continuum fit near 8 and 13 $\mu$m (Hanner et al. 1998). Filled circles: Hale-Bopp (C/1995 O1) at 0.92 AU; solid line: 1P/Halley at 0.79 AU (Campins and Ryan 1989).

Figure 10. Silicate emission features in comet Hale-Bopp (C/1995 O1). Upper curve: ISO SWS spectrum at $r = 2.82$ AU; lower curve: modelled spectrum of forsterite from laboratory data (Crovisier et al. 1997b).

Figure 11. 109P/Swift-Tuttle spectra at $r = 1.0$ AU, as observed through the atmosphere, showing emissions in excess of the continuum (DiSanti et al. 1995).

Figure 12. Mean albedo of comet dust versus phase angle in the $J$ (1.25 $\mu$m) bandpass (Hanner and Newburn 1989). The symbols are: H = 1P/Halley, C = 67P/Churyumov-Gerasimenko, K = 22P/Kopff, Z = 21P/Giacobini-Zinner, T = 9P/Tempel 1, G = 65P/Gunn, W = Wilson (C/1986 P1). Open circles are for comets observed at $r > 3$ AU.

Figure 13. Observed $J - H$ and $H - K$ colors of comets versus phase angle (Hanner and Newburn 1989). Symbols: squares: $r < 2$ AU; filled circles: $2 < r < 3$ AU; open circles: $r > 3$ AU.

Figure 14. Dust particle fluence versus mass as measured by the DIDSY and PIA experiments on board the GIOTTO Halley probe (McDonnell et al. 1991).

Figure 15. The ratios of average Mg-normalized abundances in the short and long spectra, as determined from the data collected by the instruments PUMA-1 and PUMA-2. All studies essentially agree that ions from the CHON-elements in the short spectra are approximately a factor of ten more abundant than in the long spectra, while ions from the rock-forming elements in both types of spectra are of equal abundance. We do not have an explanation why sulfur in Mukhin et al.'s (1991) study deviates from this general observation.

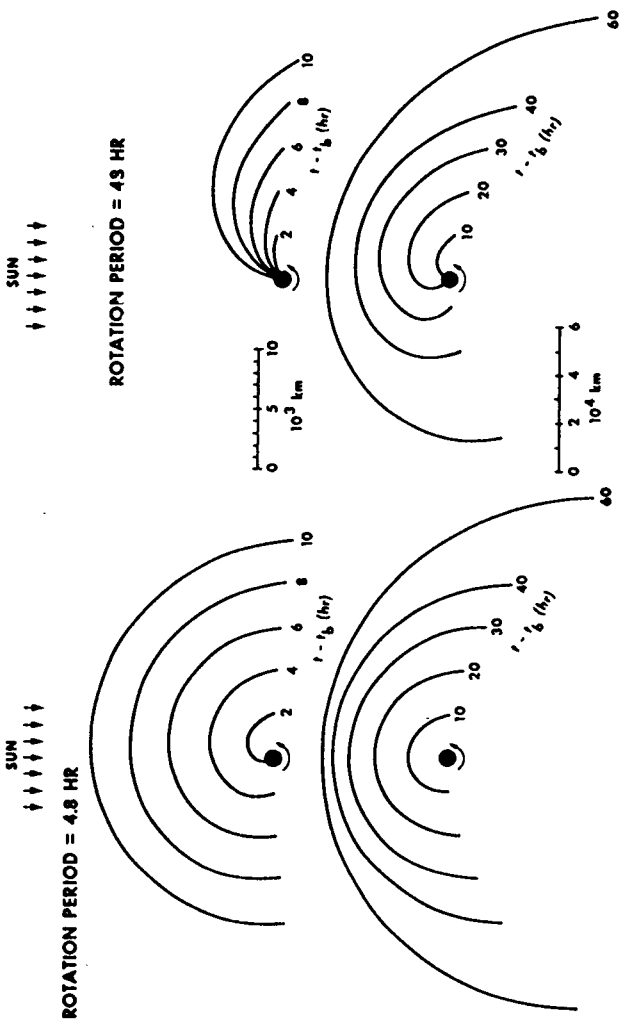
SUN
ROTATION PERIOD = 4.8 HR
SUN
ROTATION PERIOD = 43 HR
$t - t_b$ (hr)
$10^3$ km
$10^4$ km

Figure 1

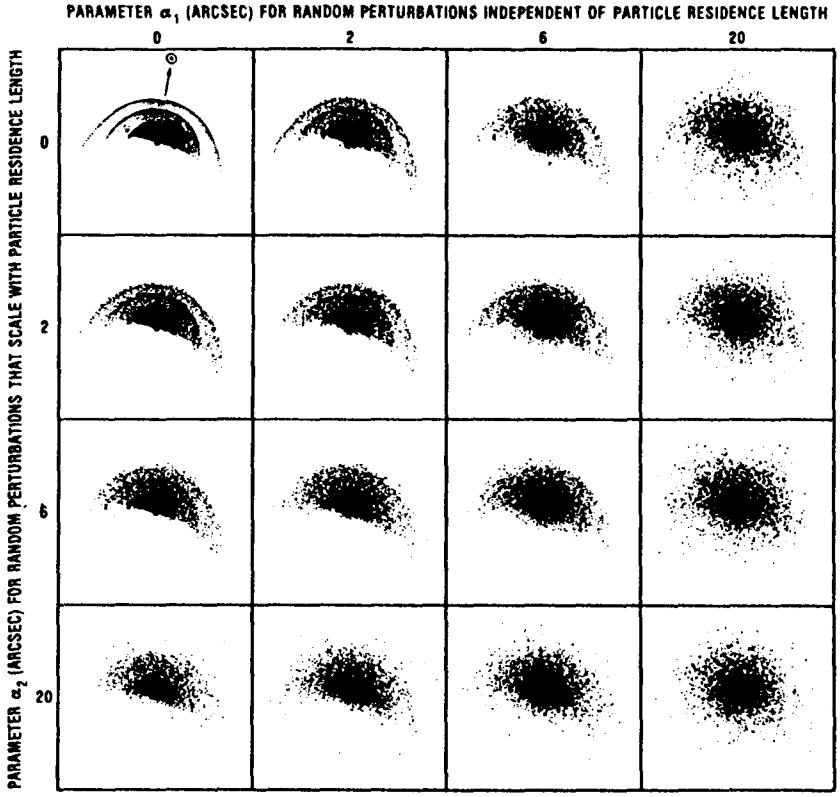
COMPUTER GENERATED IMAGES OF A SYSTEM OF SUNWARD HALOS
PARAMETER $\alpha_1$ (ARCSEC) FOR RANDOM PERTURBATIONS INDEPENDENT OF PARTICLE RESIDENCE LENGTH
0
2
6
20
PARAMETER $\alpha_2$ (ARCSEC) FOR RANDOM PERTURBATIONS THAT SCALE WITH PARTICLE RESIDENCE LENGTH
0
2
6
20

Figure 2

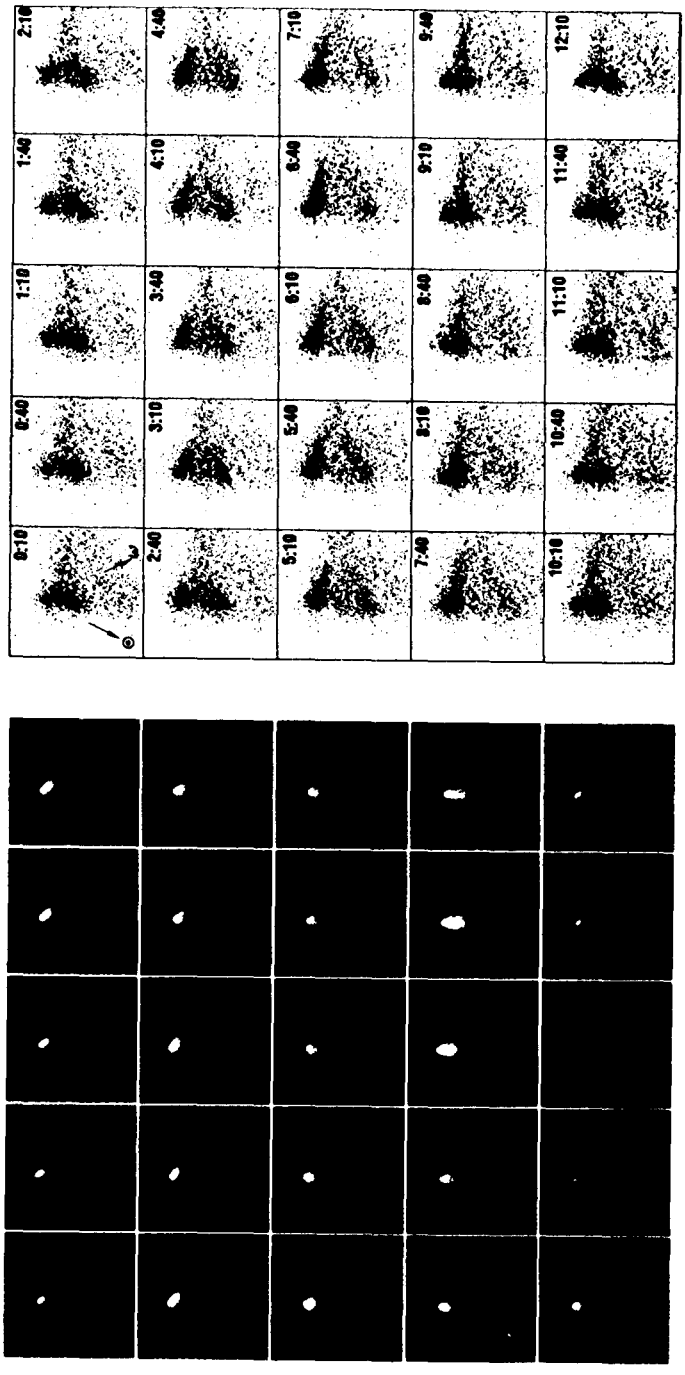
0:10
0:40
1:10
1:40
2:10
2:40
3:10
3:40
4:10
4:40
5:10
5:40
6:10
6:40
7:10
7:40
8:10
8:40
9:10
9:40
10:10
10:40
11:10
11:40
12:10

Figure 3

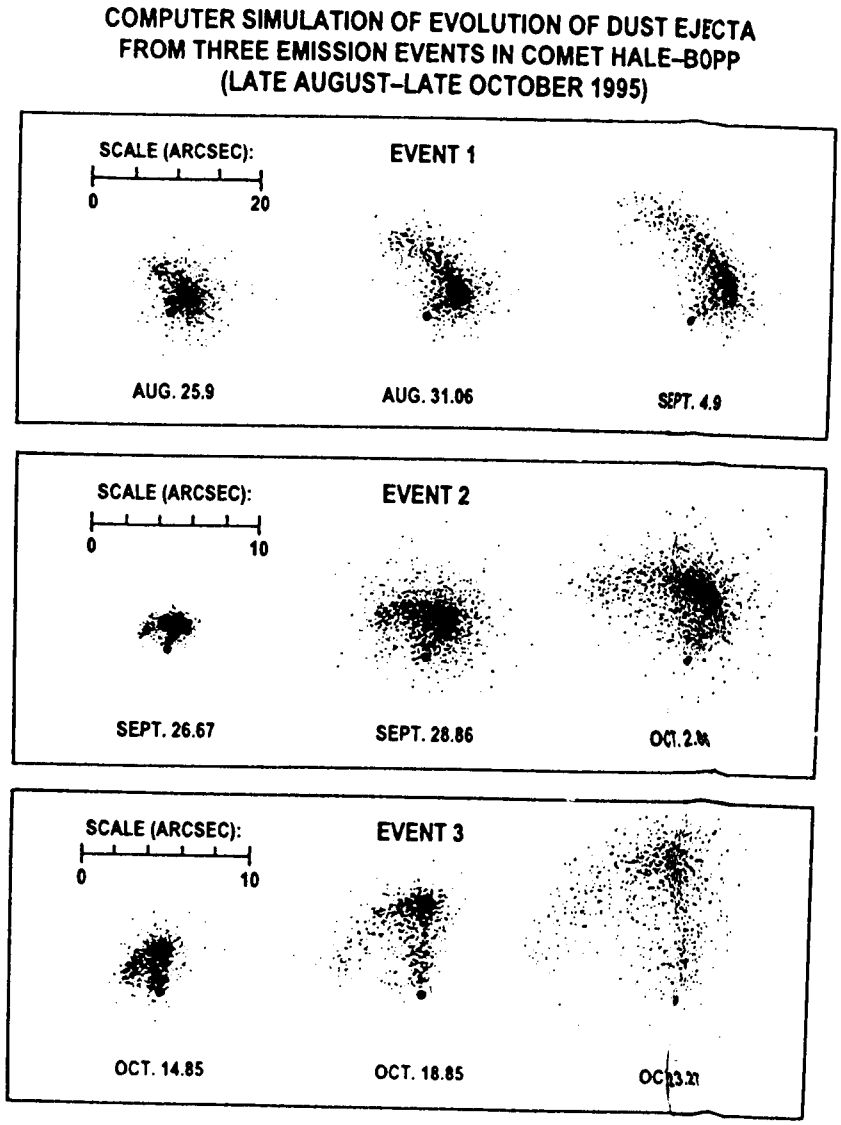
COMPUTER SIMULATION OF EVOLUTION OF DUST EJECTA
FROM THREE EMISSION EVENTS IN COMET HALE-BOPP
(LATE AUGUST–LATE OCTOBER 1995)
SCALE (ARCSEC):
0
20
EVENT 1
AUG. 25.9
AUG. 31.06
SEPT. 4.9
SCALE (ARCSEC):
0
10
EVENT 2
SEPT. 26.67
SEPT. 28.86
SCALE (ARCSEC):
0
10
EVENT 3
OCT. 14.85
OCT. 18.85

Figure 4

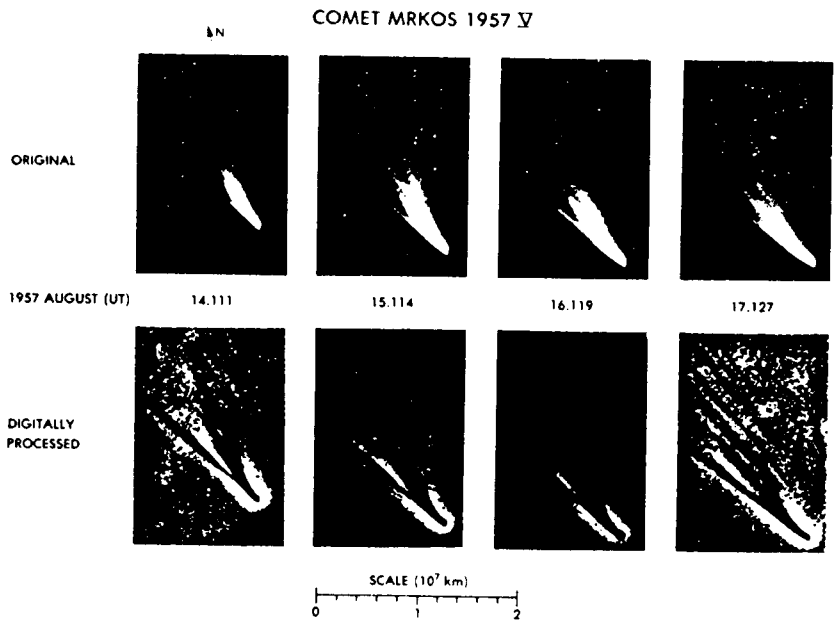
COMET MRKOS 1957 V
N
ORIGINAL
1957 AUGUST (UT)
14.111
15.114
16.119
17.127
DIGITALLY PROCESSED
SCALE ($10^7$ km)
0
1
2

Figure 5

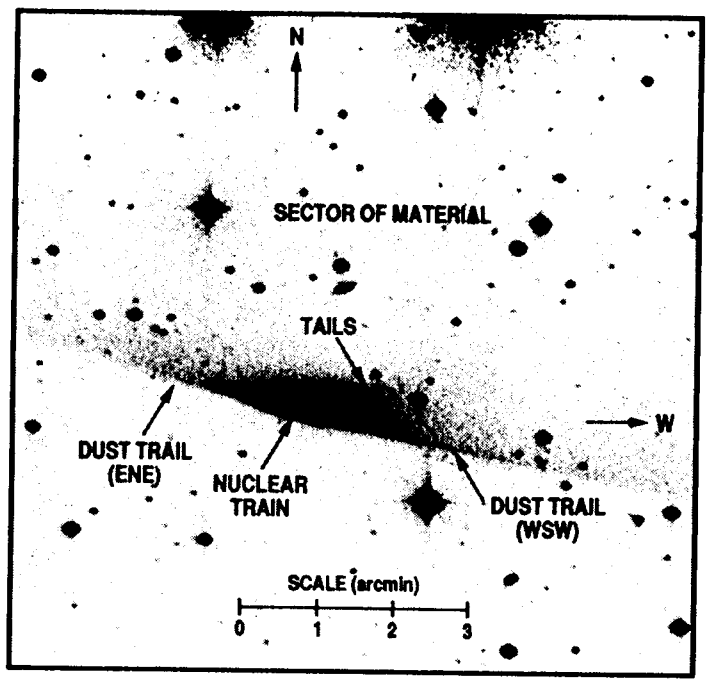
N
SECTOR OF MATERIAL
TAILS
W
DUST TRAIL
(ENE)
NUCLEAR
TRAIN
DUST TRAIL
(WSW)
SCALE (arcmin)
0
1
2
3

Figure 6

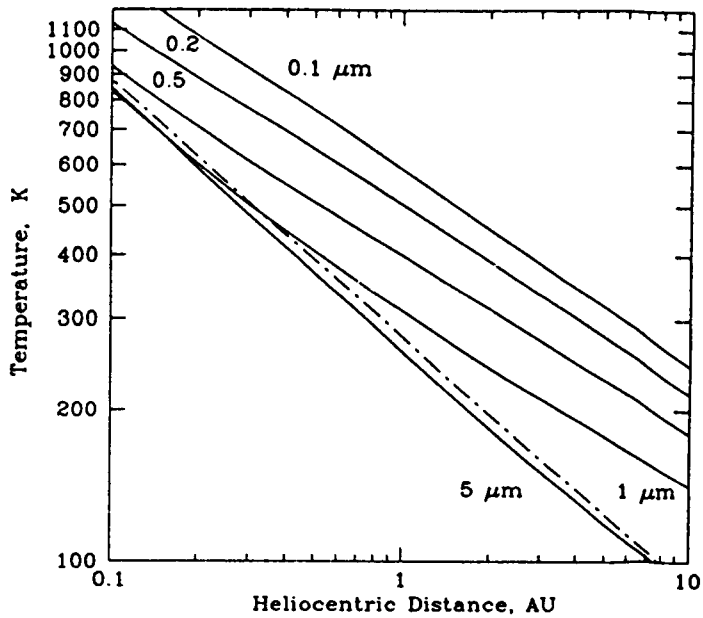
1100
1000
900
800
700
600
500
400
300
200
100
Temperature, K
0.1
1
10
Heliocentric Distance, AU
0.2
0.5
0.1 μm
5 μm
1 μm

Figure 7

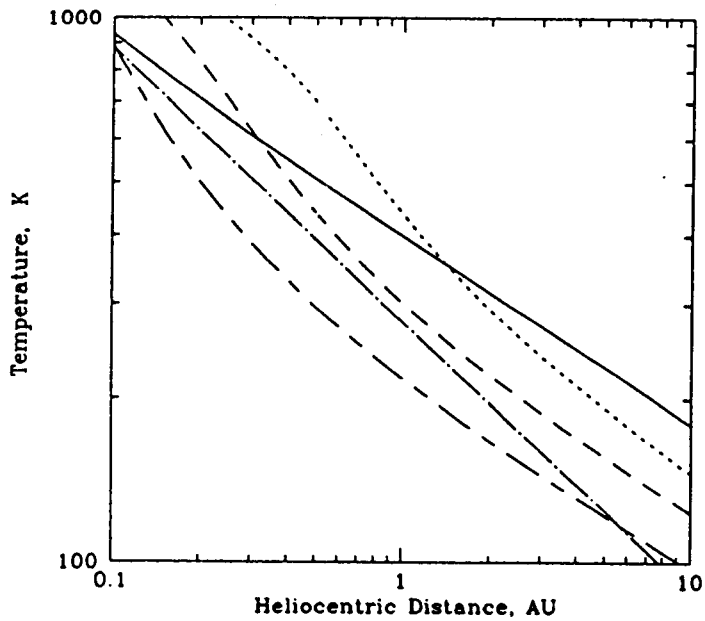


Figure 8

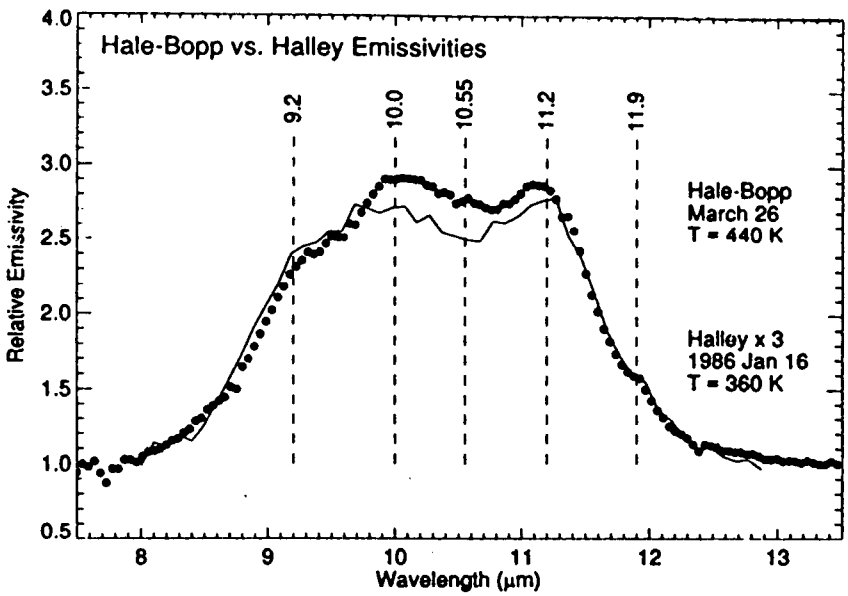
Hale-Bopp vs. Halley Emissivities
9.2
10.0
10.55
11.2
11.9
Hale-Bopp
March 26
T = 440 K
Halley x 3
1986 Jan 16
T = 360 K
Relative Emissivity
Wavelength (μm)
4.0
3.5
3.0
2.5
2.0
1.5
1.0
0.5
8
9
10
11
12
13

Figure 9

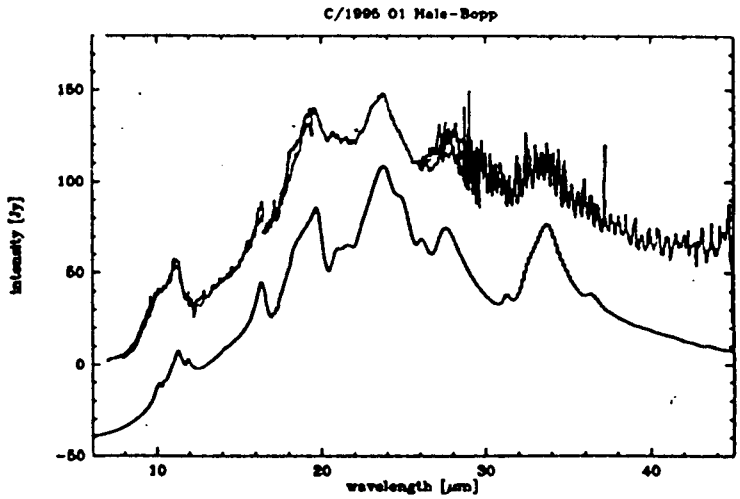
C/1995 O1 Hale-Bopp
150
100
50
0
-50
10
20
30
40
intensity [Jy]
wavelength [μm]

Figure 10

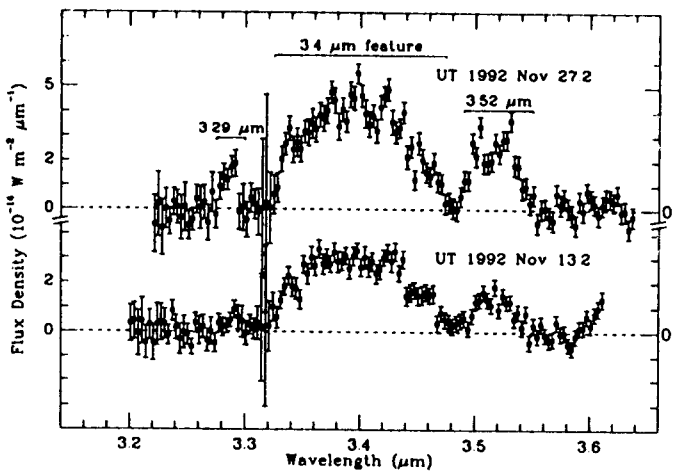
3.4 μm feature
UT 1992 Nov 27.2
3.52 μm
3.29 μm
UT 1992 Nov 13.2
Flux Density ($10^{-16}$ W m$^{-2}$ μm$^{-1}$)
Wavelength (μm)
3.2
3.3
3.4
3.5
3.6

Figure 11

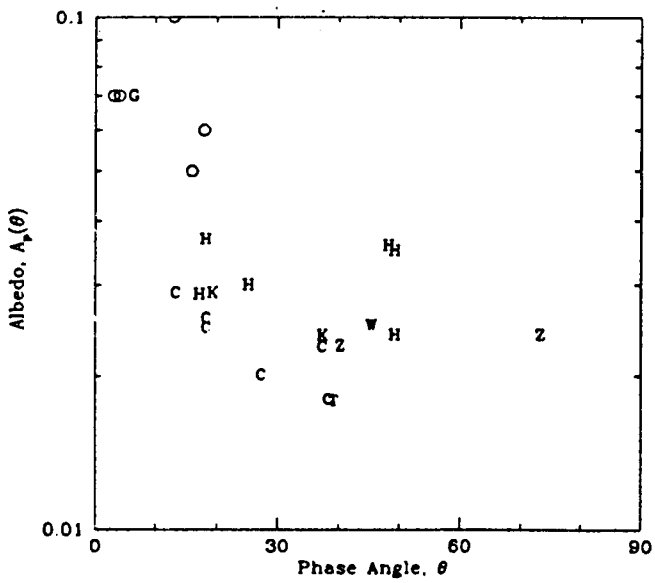


Figure 12

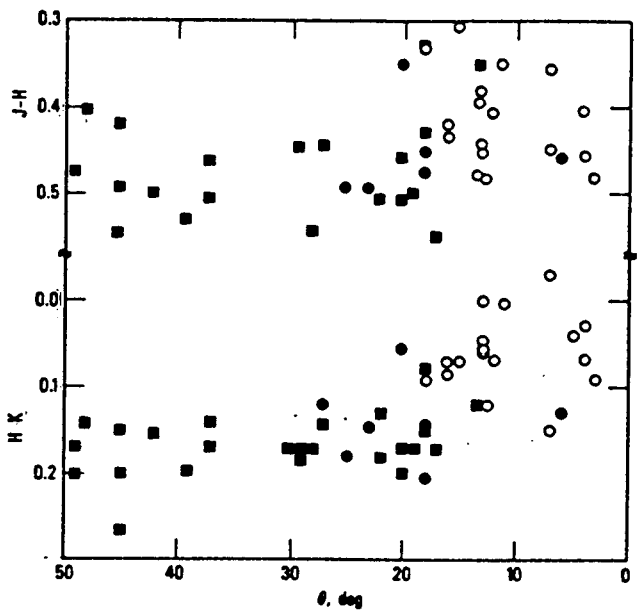


Figure 13

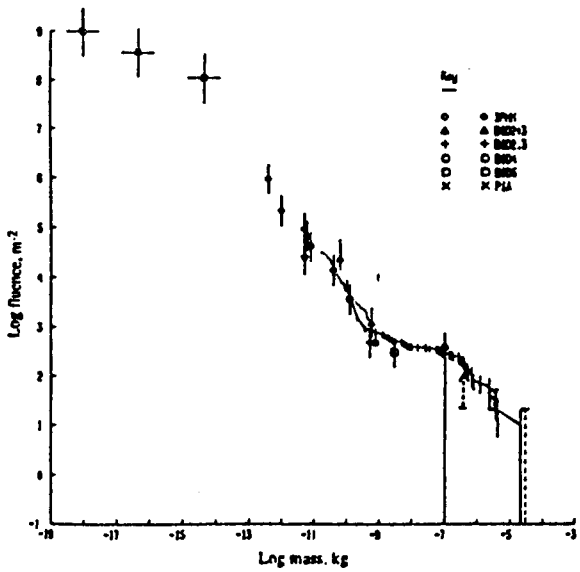


Figure 14

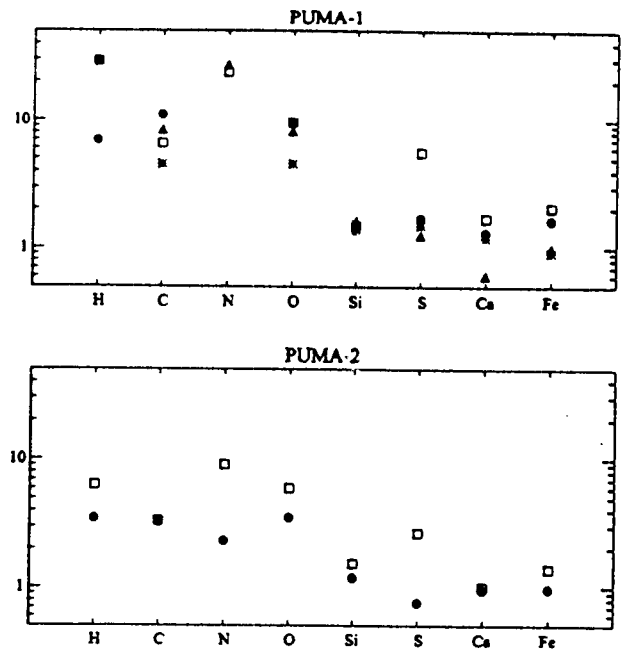
PUMA-1
10
1
H
C
N
O
Si
S
Ca
Fe
PUMA-2
10
1
H
C
N
O
Si
S
Ca
Fe
● - Langevin et al. (1987)
▲ - Jessberger et al. (1988)
✖ - Lawler et al. (1989)
□ - Mukhin et al. (1991)

Figure 15

Table 1. 10 micron and submillimeter fluxes from comets.

| Comet | $R$ (AU) | $T_{BB}$ (K) | 10 $\mu$m flux[a] ($10^{-12}$ W/m$^2$/$\mu$m) | Submillimeter flux density predicted[b] (mJy) | Submillimeter flux density observed[c] (mJy) | $\lambda$ (mm) |
|---|---|---|---|---|---|---|
| 23P/Brorsen-Metcalf 1989 N1 | 0.48 | 401 | 1.6 | 80 | 90 | 0.8 |
| | | | | 42 | 45 | 1.1 |
| Okazaki-Levy-Rudenko 1989 Q1 | 0.67 | 340 | 1.93 | 157 | 21[e] | 0.8 |
| Austin 1989 X1 | 0.57 | 368 | 2.5 | 160 | <37[d] | 0.8 |
| 4P/Faye 1991 | 1.59 | 220 | 0.3 | 85 | <7.5[d] | 1.1 |
| Levy 1990 K1 | 1.67 | 215 | 0.8 | 258 | <13.5[d] | 1.1 |
| Hyakutake 1996 B2 | 1.08 | 268 | 3.0[f] | 6000 | 550[g] | 0.8 |

[a] Data from Hanner et al. 1994a, Hanner et al. 1996; scaled to 18″ FOV.
[b] Blackbody extrapolation from 10 $\mu$m flux.
[c] Submillimeter data from Jewitt and Luu 1992.
[d] 3$\sigma$ upper limit.
[e] Mean of 6 days.
[f] Gehrz et al. 1998, March 23.3, scaled to 16″ FOV.
[g] Jewitt and Mathews 1997, March 23.5.

Table 2. Estimated mineralogical composition of Halley's dust (Schulze et al. 1996).

| Mineral group | Estimated proportion | Mineral chemistry | Possible minerals |
|---|---|---|---|
| Mg silicates | >20% | Fe-poor, Ca-poor | Mg-rich pyroxene and/or olivine |
| Fe sulfides | ~10% | some Ni-rich | pyrrhotite, pentlandite |
| Fe metal | 1–2% | Ni-poor | kamacite |
| Fe oxide | <1% | | magnetite |